T.C.

ALINBAS UIVERSITY

Electrical and Computer Engineering

VISIBLE LIGHT COMMUNICATION SYSTEM USING 4X1 WDM

Mustafa Ihsan Mustafa

Master Thesis

Prof. Dr. Osman Nuri UÇAN

İstanbul, 2019

VISIBLE LIGHT COMMUNICATION SYSTEM USING 4X1 WDM

by

Mustafa Ihsan Mustafa

Electrical and Computer Engineering

Submitted to the Graduate School of Science and Engineering

in partial fulfillment of the requirements for the degree of

Master of Science

ALTINBAS UNIVERSITY

2019

This is to certify that we have read this thesis and that in our opinion it is fully adequate, in scope and quality, as a thesis for the degree of .....

Academic Title Name SURNAME	Academic Title Name SURNAME
Co-Supervisor	Supervisor

Examining Committee Members (first name belongs to the chairperson of the jury and the second name belongs to supervisor)

Academic Title Name SURNAME	Faculty, University	_____
Academic Title Name SURNAME	Faculty, University	_____
Academic Title Name SURNAME	Faculty, University	_____
Academic Title Name SURNAME	Faculty, University	_____
Assoc. Prof. Name SURNAME	Faculty, University	_____

I certify that this thesis satisfies all the requirements as a thesis for the degree of .....

_____

Academic Title Name SURNAME

Head of Department

Approval Date of Graduate School of Science and Engineering: ____/____/____

_____

Academic Title Name SURNAME

Director

I hereby declare that all information in this document has been obtained and presented in accordance with academic rules and ethical conduct. I also declare that, as required by these rules and conduct, I have fully cited and referenced all material and results that are not original to this work.

Mustafa Ihsan Mustafa

DEDICATION

To my beloved family (My dad, mom and brother), to my teachers in the past, present and future. To my Prof. Dr. Osman Nuri UCAN, to my friends and to all those who truly believed in me and never let me down throughout the way.

ACKNOWLEDGEMENTS

I wish to express my acknowledgements to my supervisor, Prof. Dr. Osman Nuri UÇAN who was abundantly helpful and offered invaluable support with his sincerity and belief in me.

ABSTRACT

VISIBLE LIGHT COMMUNICATION SYSTEM USING 4X1 WDM

Mustafa, Mustafa Ihsan

M.Sc., Electrical and Computer Engineering, Altınbaş University,

Supervisor: Prof. Dr. Osman Nuri UÇAN

Date: June 2019

Pages: 62

A wireless technology that transmits the message by using a carrier's visible light is Visible Light Communications (VLC). Three fundamental colors, red, green and blue, show the white light. These colors are multi-colored and operate at different wavelengths with their respective colors. Different information signals control LEDs by the Wavelength Multiplexing Division (WDM) and are converted into a single optical multiplexed data stream. This optical data stream is split into distinct colors or wavelengths and is then decrypted with the image sensors with a color filter in the receiving hand. The higher data rate may be achieved from a parallel point of view thanks to WDM information. In this document, the OptiSystem software shows a 4x1 WDM based VLC scheme. The information rate achievable is up to 100 Mbps, which has a 3x10-8 Bit Error Rate (BER).

Keywords: Visible Light Communication, Wavelength Multiplexing Division, optical data, bit error rate, LED, light, Multiplexing.

ÖZET

4X1 WDM KULLANAN GÖRÜNÜR IŞIK İLETİŞİM SİSTEMİ

Mustafa, Mustafa Ihsan

Yüksek Lisans, Elektrik ve Bilgisayar Mühendisliği, Altınbaş University,

Danışman: Prof. Dr. Osman Nuri UÇAN

Tarih: Haziran 2019

Sayfalar: 62

Bir taşıyıcının görünür ışığını kullanarak mesajı ileten bir kablosuz teknoloji Görünür Işık İletişimi'dir (VLC). Kırmızı, yeşil ve mavi olmak üzere üç temel renk beyaz ışığı gösterir. Bu renkler çok renklidir ve kendi renkleri ile farklı dalga boylarında çalışırlar. Farklı bilgi sinyalleri, dalga boyunu Multiplexing Division (WDM) ile LED'leri kontrol eder ve tek bir optik multiplexed veri akışına dönüştürülür. Bu optik veri akışı farklı renklere veya dalga boylarına bölünür ve alıcı eldeki renk filtreli görüntü sensörleriyle şifresi çözülür. WDM bilgisi sayesinde daha yüksek veri hızı paralel bir bakış açısıyla elde edilebilir. Bu belgede, OptiSystem yazılımı 4x1 WDM tabanlı bir VLC şeması göstermektedir. Elde edilen bilgi hızı, $3x10^{-8}$ Bit Hata Oranı (BER) olan 100 Mbps'ye kadardır.

Anahtar kelimeleri: Görünür Işık İletişimi, Dalga Boyu Çoklama Bölmesi, optik veri, bit hata oranı, LED, ışık, Çoklama.

TABLE OF CONTENTS

Pages

LIST OF TABLES

Pages

LIST OF FIGURES

Pages

1. INTRODUCTION

Visible light communication (VLC) is a technology that enables a short-range wireless communication connection to be provided via lighting. VLC systems benefit from the license-free spectrum of light and their immunity to interferences in radio frequency (RF). The information is often transferred to these structures by modifying the yield intensity of the LEDs while the Data Signal is retrieved by means of straightforward photodiodes (PDs) at the recipient hand. Researchers at the University of Keio in Japan suggested using white LED for lighting and communication in households as part of the construction of the network of access [96]. Interest in this industry started to grow, especially in Japan, as VLC support for mobile devices and car communications increased as a basis for high-speed communication via visible light. That resulted to the creation in November 2003 in Japan of the Visible Light Communications Consortium (VLCC). By 2007, VLCC suggested two norms which were subsequently approved as JEITA CP-1221 and CP-1222, respectively, under the Japan Electronics and Information Technologies Association (JEITA). The requirements and indicator level needed to avoid interference from various VLC devices are determined by JEITA CP-1221 only, and a visible Light ID system defined by JEITA CP-1222. In the meantime, also as a chance to enhance communications capacity within the RF network under EU Framework Project 7 (FP7) was introduced the European Commission's Home Gigabit Access Project (OMEGA) [91], and the IEEE initiated the standardization process in 2008.

The 2011 IEEE 802.15.7 [62] standard was a major move towards marketing and extensive VLC network deployment [54, 55]. Only the physical (PHY) and medium access (MAC) layers are defined. It proposes three methods of physical layer. PHY I is for external use, whereas PHY II and PHY III are for indoor application. Thirty modulation and coding combinations are indicated in total. For forward error correction (FEC), PHY I uses Reed-Solomon (RS) and Coevolutionary Codes (CC), while PHy II and III are mainly dependent on FEC only. On-offkeying (OOK) and pulsation variable (VPP) modulations are used by PHY I and PHY III, whereas PHY III uses only the color shift key (CSK). Thus three modes provide different rates for both the modules, PHY I, PHY II and PHY III, which are based on the modulation choice of the Run Limited (RLL) code, the Optical Clock Rate and FEC Code, for a rate of 11.67 to 266.6 kbits / s, 1.25 to 96 Mbps and

12 to 96 Mbps[100] respectively. The Mac layer covers the following features: 1) mobility support, 2) dynamic support, (3) visual support, (4) color reduction, (5) color support, (6) network beacon produced by the unit coordinator, (7) disbanding and support for the Visible Light Communication Personal area (VPAN) network linking between peer MAC organisations, respectively. Mac layer is a comprehensive network network support. The application layer is postponed for security factors. Note that the 802.15.7 layer of MAC is very near to IEEE 802.15.4 MAC [93] wireless personnel area network. Pair-to-pair, broadcast and stellar the topologies backed by the MAC layer. In the topology of the stars, all the nodes interact via a central control unit. Within the topology peer-to-peer, one of the two nodes that communicate with each other plays a controller position. Three device classes are taken into account: cars, mobile devices and infrastructure. However, these norms do not take account of many VLC instances and VLC techniques. Additionally, according with application environment specifications, VLC devices can use other light source and light sensor types. This is why in the end of 2014 a revision of the IEEE 802.15.7-2011 standard has started with the IEEE task group 7 m, first published as IEEE 802.17.5r1. The modification of IEEE 802.15.7 m is to be published by 2018. In reality any light sources that change states at a high pace can be used as transmitters for VLC devices (i.e. the transition between ON and OFF). The screens, as proposed in [72, 49, 59, 71], can therefore also be used as transmitters. The barcodes or QR codes displayed on a screen are used to encode data by these methods.

HiLight [71] is a fresh way of connecting screen to camera that encodes information into translucent pixels. Without hindering the picture or video displayed, this technology can communicate data effectively. A VLC receiver could be used for any device that detects the existence or lack of visible light. Because of their quick reaction and elevated bandwidth, most research is concentrated on using PDs as receivers. Works such as [97] indicate that frequent LEDs can work as recipients in reverse bias mode, but that they are sensitive to PDs in comparison. The high frequency light patterns mentioned in [22] can also be detected through smartphone cameras. In summary, the VLC emitter can be 1) the modular LED, 3) the passive light, such as incandescent lights and fluorescent light pipeds, 2, 3, and often colored LEDs. For its portion, the VLC receivers are 1) specifically designed photodiodes for sensing light, but also 2) LEDs for lighting and lastly the 3) cameras.

Table 1.1: VLC systems classification

	PD	Small Color LED	Camera
Flashlight			
Lighting power LED			
Small Color LED			
Screen			
Passive			

1.1 PURPOSE AND THESIS IMPORTANCE

The idea of this study is to have the optical data stream divided into different colors or wavelengths with color filters in the receiving side and is then decrypted with the image sensors. Due to the WDM information, the greater data rate can be obtained parallel perspective.

2. LITERETURE REVIEW

2.1 PHOTODIODE AS VLC RECEIVER

2.1.1 Ceiling LED-to-Photodiode Communication

Modulation: The easiest way of allowing high velocity VLCs is the LED-to-photodiode. While current VLC standards cover OOK, VPPM and CSK modulation with information rates less than 96Mbps, considerably greater manufacturing in laboratory circumstances is possible and proved. The use of familiar RF or optical fiber alternatives is a simple strategy to improve the data rate. In order to obtain a bidirectional in-time transmission of a complete speed of 230Mbps, the prototype VLC scheme with high-performance LEDs and OOK was introduced by pursuing this route [21]. A complete duplex bi-directional VLC system, based on the use of RGB LED and marketable phosphorous LEDs, is suggested in [27] inspired by optical fiber communications. In order to achieve the bidirectional transmission, the authors used Wavelength Division Multiplexing (WDM). In addition, Orthogonal Frequency Division multiplexing (OFDM) and QAM were used to boost the performance [5]. Due to its high spectrum efficiency and its ability to mitigate inter-symbol interference (ISI), OFDM was commonly used in wired and wireless communication systems. The VLC system has enhanced its velocity when using OFDM in VLC to [17] 3.75 Gbps, compared to the downlink of 575 Mbps and the uplink of 225 Mbps. In latest years, the potential of OFDM was further explored. Consisting of particular VLC characteristics, several OFDM (Acco-OFDM)[64] (ACO-OFDM)[8] (OFDM) and the AC-Biable OFDM (ADO-OFDM)[27] asymmetrically cut were created for the particular characteristics of VLC. Initially, the DCO-OFDM was implemented for wireless infrasound optical communication [64]. This provides the analog bipolar signal with a DC bias and clicks on other negative values. When the DC biazon is set to a large standard the optical signal to noise rates (SNR) will be very high. This results in a low optical efficiency. The DCOOFDM disadvantages were therefore being suggested by ACO-OFDM. Only strange sub-carriers are transmitted data from ACO-OFDM. In addition, clipping noise is only added to even subcontractors, so that data on unlikely subcontractors will not interfere. This increases DCO-OFDM's energy effectiveness, but leads to a small spectrum performance of half DCOOFDM and one-quarter RF OFDM. ADO-OFDM is suggested for

mixing ACO-OFDM and DCO-DM in [27]. OFDM is transferred in the scheme on strange subcontractors and it is transferred by DCO-OFDM on equal subcontractors. In the process, ADO-OFDM exceeds the power efficiency of the DCO-OFDM and exceeds the spectrum efficiencies of the ACO-OFDM. These modulations are at the backdrop of LiFi and the ready-to-market LiFi and USB access pointsPureLiFi LiFi-X [96].

MIMO: The attocell architecture was suggested for the provision of both lighting and continuous interaction [78]. Each LEM bulb is considered as an access point and light source in the LiFi network. This attocell architecture can be based on a good multiinput multiple output (MIMO) technology, called spatial modulation (SM). For RF communication in [15], this MIMO technique was initially suggested, when at any moment only one transmitter transmits information. Fath et al. tailored RF SM additionally for VLC [35]. A special symbol is allocated to each Sender LED and the LED is enabled when the information to be transferred corresponds to the symbol. The receiver estimates and uses the LED activation to decode the transmitted data on the basis of the signal. In [34] the authors showed that SM provides high spectral efficiency, which can be robust and linked. In latest years, SM was researched more closely [83, 25] due to the benefits shown in [34]. Networking many works on the VLC from the viewpoint of the PHY layer, disregarding media and networking. In fact, to allow VLC networking and VLC deployment, it is essential to build robust and efficient media sharing protocols. For accessing and downlinking, consumers in the attocell architecture have to be linked to one or more LED lights and can switch from an access to another by using horizontal handling processes. In [19] we reviewed the model and effectiveness metrics of user mobility such as the download of files and average connectivity. However, VLC-uplink transmission remains challenged: an optical uplink may interfere with the downlink signal, a computer's optical uplink can be difficult to use or the increased electricity usage can make integration impractical. For these purposes, LiFi uses IR for the uplink [47] to exploit these issues. The VLC and current RF network can also be combined as WiFi [97, 60, 74, 110, 19]. In [97, 60], where the VLC is only used in broadcasting, the VLC indoor integration scheme is suggested. Nevertheless, these hybrid systems involve WiFi to handle VLC frames ' uplink recognition, which often results in small packet traffic. The findings of their simulation showed that this strategy decreases only WiFi device performance [97]. The other insight is that the VLC latency and

transmission rate are adversely affecting these WiFi equipment. These issues must be explored further.

The primary challenge for hybrid VLC networks, even with moving stations, is the vertical transfers between LiFi and WiFi. In a hybrid system where optical bindings can be blocked, Hou and O'Brien [54] suggested a flexible vertical handover decision-making algorithm. Depending on the blocking time, the system is transmitted to an RF network. Vegni et al. [20] are introducing signal strength (RSS) based transmission methods similar to the RF transmission protocols. The writers also launched a new mobile station protocol in which provides effective vertical and horizontal handling processes for a LiFi and WLAN hybrid network.

Other concerns: One important VLC issue is what happens when LED lights turn OFF to data communication? A fundamental response is that there is no communication anymore. Indeed, the above-mentioned works took for granted that lighting is turned on. Nonetheless, some scenarios exist where people don't want indoor lighting just before or during sleep, as in sunny days or during the night, while network connectivity is still required. This is the case for intelligent home situations in which intelligent thermostats send temperature information or IP video streaming cameras. Tian et al. suggested the DarkLight [97] to tackle these scenarios in which VLC and no visible indoor artificial lighting have to co-exist. When LEDs are very weak and not perceptible to humans, the light depends on DarkLight. To this end, DarkLight modulates the LEDs with 500 ns light pulse and a 0,007 percent LED cycle. Then 12PPM modulation will encode information. Note that the device must have a highly accurate timepiece in order to obtain and interpret the pulse position in a nanosecond scale. That is why the writers use FPGAs and an expensive PIN photodiode to introduce darklight on the test bed. The experimental assessment shows that DarkLight reaches a data rate of 1,6 kbit / s and promotes a communication distance of up to 1,3 m, while maintaining the sensitive light negligible.

Ceiling LED-to-photodiode for localization: Location indoors is a prevalent area of application for communication from LED to photodiode. As the enormous deployment of IoT devices is often a main element in precise placement, there is an ever-increasing interest in locational services. GPS has mainly fixed the outdoor scenario issue. However, precise location for indoor settings is still a challenge. The benefit of low deployment costs due to the use of WiFi transceivers and the current

WiFi infrastructure has been drawn to a wide range of study projects through WiFi, however, its precision continues as small as few feet [11]. However, VLC has no disadvantages of dynamics, fading, interfering or multipath-like wireless channel radiation. In [70], Epsilon was launched to deliver a decimeter of precision indoor localization, leveraging LED lights and any photo-diode fitted device. The LED ceiling anchors serve as an identity, place and cycle of operation. Epsilon is able to use binary frequency change controlling keys to ensure the accurate transmission of multiple and uncoordinated fuels, along with hopping frequencies from the receptor, which then measures LED rss in the field of perspective and calculates the distance to them using a channel pattern. Finally, its position is calculated by using light sources and trilateration range measurements. The accuracy of the scheme was confirmed by experimental outcomes: For the three typical office surroundings with 5 LEDs the 90th percentile precision is 0.4 m, 0.7 m and 0.8 m. However, the reliability of this process is still poor and the system is not robust against the device or the moving system and channel model efficiency is linked to accuracy in distance measurement.

Ceiling LED-to-photodiode for sensing: Indoor environment user experience and entertainment have been enhanced by recent developments in increased reality and intelligent home equipment. Common and commercial methods use cameras (RGB, infrasound or flight time cameras), sensors, radio frequency signals in the atmosphere and sound signals to feel free-hand gestures. For the first time, the writers suggested in [7] using light to detect body movements and to identify users. The system comprises of LED lights on the roof with VLC-enabled lamps that emit light lamps on one hand and PDs on the ground on the other. The PDs capture an ongoing stream of LED light-every shadow maps. In this shadow map, the body joints of the user can then be found in a 3-dimensional room and the user is defined based on calculated body parameters like shoulder width or arm length. Experimental results show that 8 of 10 individuals with a mean body parameter estimated to be 0.03 m are correctly identified. In Aili [73], a supplementary scheme is suggested using a table lamp for the real-time reconstruction of the 3D skeleton. Aili comprises of a multi-array LED panel of PDs integrated in the base lamp. To restructure a hand skeleton Aili combines light block maps from individual PDs to demonstrate whether a Hand blocks light rays from individual LEDs to all pds. Each light emitted a distinctive blinking frequency from 20.8 kHz to 40 kHz in order to recognize the contribution of a certain LED. The writers created and assessed

their system's prototype. The results show that your algorithm rebuils a hand with an average angular deviation of 10.2 ° and a mean translation deviation of 2.5 mm within 7.2 ms. The cost and deployment complexity of these works is also at a disadvantage on the sensor hand. This problem makes the solutions incompatible with the IoT sensor limits, which must be kept in cost, energy usage and integration complexity as small as possible.

2.1.2 Low Power LED to Photodiode Communication

Most study on communication between LED and photodiodes aims at achieving high-speed communication. Some instances of use, however, do not require a high data rate. This is true of the IoT context in particular. Indeed, it takes just few parts or no kilobits to interact with intelligent objects or to collect sensor valuesThis can be seen in [21] where a user on a smartphone interacts with smart toys. As smartphones do not incorporate a photodiode today, the author utilizes an audio jack to plug a small VLC board with a PD and LED. In HiJack [67], the author introduced this strategy first where heart rate sensing abilities are transferred to an unmodified smartphone. The unit is driven by the output signal of the jack and no further battery is necessary. The audio signals modulate the LED's light emissions, while a photo diode detects the incoming light. The VLC clock speeds of 10 kHz are helpful for an audio sample speed of 48 kHz. The electric signals produced are fed into the microphone input and a mobile telephone application ultimately demodulates the audio-like signal. The Author scheme was implemented on an iPhone, and the test results showed, for a packet size of 150 bytes, that the output is stable up to 25 cm and maximum 700 bps. Almost all smartphones now use a camera, as consumers rely greatly on their smartphones and technological developments. As a consequence, several of them have an LED torch. There is therefore an outstanding issue to use smartphones such as a VLC emitter. The writers used the smartphone LED flashlight in [40, 38] to replace magnetic cards in a safe visible light. After showing that non-return-to-zero (NRZ) modulation systems are ineffective in information processing, they use an OOK modulation to return-to-zero (RZ) since they are susceptible to syncing difficulties. The experimental assessment using rooted Android smartphones and a PD as recipients demonstrates that up to 500 bps can be error-free. However, the writers reduce the scalability of their scheme by using a rooted smartphone. In fact, root permit applications cannot be spread via standard shops. Finding root permissions that is not the case with

most smartphone users also means that customers need to familiarize themselves more with the smartphone operating system. It should be noted that smartphone rooting has many inconveniences: the device is more susceptible to malware or data leaks, and disabled its security. Given the radical restriction of bit rate on portable operating systems and the API supplied by the software development kit (SDK), many initiatives try to improve flash lighting communications. However, the upcoming IEEE 802.15.7 m standard [61] will include VLC flashlights.

2.1.3 Passive Lights to Photodiode Communication

Wang et al. [26, 25] is presented as Passive VLC sensing as a fresh study paradigm inspired by the RF Backscatter [77]. The authors present other study problems and directions with the aim of developing a fresh sensing and communication method, using passive lights like the Sun and/or passive recipients (e.g. external object surfaces) such as fingers and car roofs. Study the channel of these specific VLC system, while [25] presents a taxonomy, and highlights three primary issues: (1) the need for more versatile and robust acceptance techniques from uncontrolled transmitters, (3) monitoring passive objects needs elevated receiver density, is not universal, as the object shape is uncontrolled. The writers categorize the scheme as full-active, passive and passive source. In [19] a latest study is provided in this sector. For detecting and acknowledging patterns of hand gestures by visible light, the writers constructed a battery free receipt. Their system utilizes battery-free energy harvesting by using solar cells that allow a low-μW electricity usage. Indeed, the complete passive architecture of the light infrastructure does not require any modification. In order to convey sensing and hand-gesture data by RF to a distance of 330 meters, they use especially the RF back scatter.

2.2 LED AS VLC RECEIVER

PDs are the finest electronic components for sensing and light receipt, because they are most used as VLC recipients. It works by turning photons into present ones. In this job, we mean pds especially designed as light recipients when we speak about pds. In [26], however, the writers suggested that standard LED be used as photosensors in the application for VLC for the first time in literature. They depend on the reality that LEDs and PDs are closely related. LEDs are both semiconductors and LEDs are manufactured for technical reasons for illumination reasons. Thus,

the LED produces a very small current by reversing an LED. Even if the intensity present in a PD is insignificant, the amplifier circuits and analog filters may be used to improve it. A cheap photo detector can be produced from an LED, otherwise the anode is bundled to the ground and the cathode is connected with a extremely driven I / O controller. The diode is reversed and its internal capacity is loaded. The I/O pin is then shifted to Input mode and the photocurrent can release the digital I / O pin of the MCU. Lastly, when you calculate how long the photocurrent is required we will evaluate the amount of incident light. Drawing on this, Dietz et al [26] proposed that LEDComm is the first two-way communication protocol LED-to-LED. The data is encrypted with pulse width (PWM) modulation: 0 is a short pulse light, 1 is a long pulse. In a limited amount of centimeters in the up and down link their prototype achieved 250bps. Following the initial demonstration, Giustiniano et al. [42], and Corbellini et al. [21] have further investigated and reinforced LED-to-LED communication. In [42] the writers improved significantly on the above-mentioned work [26]. Contrary to Dietz et al., on-off-Keys and Manchester on the physical layer encodes and decodes a signal. The authors generate an efficient CSMA / CD protocol [20] that enables the MAC layer to remove light glimpses. The protocol is accessible in French as well.

This is followed by the flicker elimination system. It is divided into symbols of Data (D) and Energy (E). The receivers and the issuers shall use both e symbols if necessary to compensate for the flicker: they shall emit light for a period of E only while the emissions emit light for a time of D and ultimately for E when the light emitted during D is insufficient. The same pattern is dispatched when the channel is idle. This job will make it possible for the first time to set up a firm two-way LED-to-LED network with up to 4 LEDs. The writers apply it to a toy prototype network that shows that their system delivers 870 bps in a range of 90 cm. The LED colors (yellow, green, blue, red) are also evaluated, demonstrating that red LEDs are at best. The color influences the LED's internal resistance and capacity and thus the downloading cycle time. In addition to the relevant element of the visible spectrum, yellow and green LEDs are better susceptibility to ambient light. OpenVLC is a networking platform with open-Source software for LEDto-LED prototyping with the communication of LED to Photodiode. OpenVLC depends on low-cost electronics and depends on the BeAglebone Black, an integrated Linux board that is plugged by a' cape' on the VLC frontend. OpenVLC provides a Linux kernel driver to sample, symbolize, code, decode, sensor, and communicate with the web layer of the Linux OS. Modulation and coding of

Manchester [42] are the foundation of the PHY layer. The CSMA / CD or CSMA with collision prevention (CSMA / CA) [20] forms the basis of MAC. OpenVLC's first version provides an MAC layer data rate up to 1 m at ranges of 2.2 kbit / s. The writers then continued to enhance the MAC layer by further changes and research. Some scientists propose CSMA to the network which uses only one LED to pass on the protocol Colision Detection and Hidden Avoidance (CSMA / CD-HA). The CSMA / CD-HA permits intra-frame bidirectional transmission in up to 4 nodes in the network. The primary goal is to use intra-frame data symbols to introduce a "LED OFF" Light emission-free embedded communication channel. A device, called R, can transmit signals to the reception of a frame parallel by means of a two-way inter-frame transmission. As the "LED ON" symbols form part of this signal, they can be felt with R com nodes. Therefore, during these nodes frames are not sent to device R and the possible issue of hidden nodes is prevented. This approach enables additional data in the same optical channel to be transferred and makes communication robust for different kinds of field of view (FOV). Writers implement the OpenVLC driver CSMA / CD-HA protocol and test results show that hidden nodes can lead to a 100% reduction in accidents and network capabilities. Galisteo et al. [41] finally introduces OpenVLC 1.2. The platform's principal shift comes with the operation of the BeagleBone Black Board's Programmable Real-Time Units. VLC demodulation has been transmitted to PRUs from Linux by the author. The PRUs are programmed in the assembler and make hardware control accurate and faster. This raises the achievable OpenVLC output to 100 kbit / s, i.e. by 8 compared with previous versions, without the need to add hardware. We observe that PurpleVLC[136] proposes a comparable strategy. The FOV of the LED is restricted with [42] to the LED axis direction. This limits its coverage to a specific direction. In[65] the authors planned to overcome this limitation by using an LED front with 20 LEDs on a circular printed circuit board. The LEDs are also spaced in Shine [65], providing 360 ° coverage. This front end benefits from having a multi-LED VLC device communicating in distinct directions with several nodes, allowing a VLC multi-hop network. Compared with current systems. Shine is a PCB based on many low-cost evaluation boards, including Beagle-Bone, Arduino and Raspberry Pi. These prototyping platforms allow rapid development of the VLC scheme at a low cost. The hardware, such as the MCU frequency, however, limits its efficiency, allowing it to only be used in small data rates modulations with low complexity. These VLC devices, however, fulfill IoT communications demands and can therefore become an indoor IoT technology. Likewise, a

recent survey shows that an LED with light power works as a light sensor. The sensibility of the LEDs used by [26, 42, 107, 108] is however significantly weaker. The LEDs array and process adjustment in Yang et al.'s solution [26] add an analog amplifier to modify the circuit systems to make sure that the signal is sensed without inverse LED bias. This problem has also been solved. This sensor-capable light infrastructure was used to deduce both occupancy and occupant motion. CeilingSee perceives light reflection on the earth and uses a pre-processing process to prevent noise with smoothing to determine occupancy using a Vector Response Support model-based learning method. The writers performed comprehensive laboratory experiments. The findings indicated that CeilingSee can even in dynamic situations determine the amount of occupants in a 30 m2 space with an occupancy of more than 80%.

2.3 SCREEN-TO-CAMERA

The enhanced number of cameras and screens offer a good opportunity to use this communication system in today's environment. This screen-to-camera links are characterized mainly by their highly directional nature and enabling wireless communication without interference. The screen for the connections to the camera is visible because both screens and camera convey a Multi-Input and Multi-Output (MIMO) communication channel, each pixel being an antenna. As a two-dimensional transmitter and receiver respectively Screen-to-camera communication therefore has the ability to offer a greater performance than LED-to-camera communication in general broadcasting communications. Nevertheless, it is difficult to enable Screen-to-Camera communication. The writers are presenting an information transmission scheme on LCD-to-camera connections in PixNet [95]. To fix the LCD's camera connectivity, PixNet utilizes OFDM transmission algorithms, i.e. vision distortion, bubble and ambient light sensitivity. In fact Pixnet is a 2-D type of barcode, but PixNet does not encrypt data directly into the visual domain, but encodes information in the frequency domain. The strategy is comparable to OFDM, but PixNet encrypts information in 2-D space frequencies, as opposed to RF-based OFDM, which codes information in time frequency. Perli et al. [95] used LCD and cameras from outside the shelf to implement PixNet. Experimental assessment demonstrated that their system provides up to 12 Mbps of throughput at 10 meters and is operating with view angles as broad as 120 °. In COBRA

[49] another way to communicate between screen and camera was provided. COBRA is intended for communicating with smartphone cameras using 2D barcodes between tiny screens. The initial information is added with a header and the CRC check sum. Then each byte in the information block is encoded in a particular color and then displayed on the screen. The barcode is divided into three sections: 1) Edge Tracker, 3) Central Code Region and 2) Timing blocks. The trackers of ground (1) are used to set the barcode on the screen with red or green blocks in the left and bottom right corners and with purple blocks in the other two angles. You can also use the smartphone to identify reference blocks for black and white time (2). These time blocks (2) are used as a reference in the area of code for the detection of data blocks (3). Data are encoded in the code zone by the color sequence blocks, where00, 01, 10 and 11 are represented by red, green, blue, and white colors. This means that 10110001 is coded according to COBRA bit-maping in blue-white-red-green blocks. At the receiver COBRA chooses the highest value for each barcode for further processing and decoding because the camera frame rate is greater than the barcode frequency. The findings of experiments indicate that COBRA has a capacity of up to 172 kbit / s. LightSync [58] further expanded the restricted accessible throughput in screen-to-camera connections. By improving the framework sync between transmitter and receiver, Hu et al. [58] almost doubles the achievable COBRA output. To recover lost frames, LightSync utilizes linear erasure code. Color tracking then is used for correctly decoding incomplete frames data. Another code-set called Styrofoam [76] discussed the ISI issue by inserting vacant frames into the produced frame set, owing to a absence of synchronization. In recent times, HiLight has launched Li et al.[71] a fresh technique for communicating between screen and camera without pictures coded. With the characteristics of the channel known as the alpha channel, HiLight incorporates the parts by changing the pixel transparency rather than altering the RGB channel colour. The transmitter uses BFSK, where bit 0 and 1 are represented by multiple frequencies through a certain number of frames. HiLight can reach up to 240 bps via off-shelf smartphones. Du etc. [30] implemented the channel-coding technique SoftLight to improve the strength of the above screen-to-camera system, which automatedly adapts the data transmission speed to connection features in distinct circumstances. SoftLight enhances the state of the art in relation to the present barcode system by offering color modulation schemes which provide a clear indication of the frequency of the Bit Error (BER). This means, if a bit can be deemed confident or not, the recipient will discern. Instead

of a packet erasure channel a bit level VLC erasure channel can be set. For the low calculations complicated transmissions, the author was able to build a rate-free coding scheme. It can be installed on all bar code layouts, including QR code or COBRA [49] and on the previous monitor, SoftLight is on-screen coding systems. Its scheme uses the separate parts and a particular color set within YUV to minimize interference between neighboring symbols to enhance the picture color conservation. The light-weight bit rate-free coding scheme first codes information with FEC code, such as Reed-Solomon (RS) or LDPC code, to create an unpredictably high-speed framework before XOR activities are carried out at frame level. The smartphone decodes the image on the recipient hand through inverse activities. The mild hint of the color modulation can then determine the possibility of mistake for each bit position, which enables for uncoded level coding. In addition, an algorithm for majority voting is used to reduce the effect of elevated probability error bits. Experimental evaluations of Android smartphones have shown that the approach correctly transmits 22 kB in 2 smartphones in less than 0,6 s and raises the average COBRA production by 2,2[49]. As screen-to-camera links for close-field communication become increasingly popular, the safety aspects of the channel are becoming indispensable. Zhang et al. addressed screen-to-camera security issues and proposed improving screen perspective and user motion tracking.

2.4 LED-TO-CAMERA

Efficient and high-speed data links are created in most VLC research. LEDs are used because pds deliver high bandwidth and fast reaction that can support highly effective and complicated modulation systems. However, when high performance is not needed, smartphones can also be used to receive VLC systems. Danakis et al. [22] demonstrate that the smartphone cameras ' so-called rolling shutter mechanism can capture models in more detail following quick modulation of light sources. The camera can be used as a VLC receiver for data transfer and data location using this scheme. In fact, Rajagopal et al. [99] are using BFSK as an iOS receiver with a capability of 10 bps up to 1 m. The authores of [22] used encoding systems from OOK and Manchester, using a framework rate of 20 fps and achieving a dataspeed of 1-3 kbit / s nearly 9 cm. The frequency shifting key (FSK) module RollingLight [68] reports a capacity of 90.56 bps, with an illumination of 60 cm x 60 cm, from an iPhone 4 receiver to a range of 1.6 meters. Schmid et al. [106] recently supplied a Pulse Position Module (PPM) encoding scheme for outputs of more than 1.2kbit / s.

Their receiver had a frame rate of 240 fps and a maximum range of 2.75 meters on the iPhone 6s. All these projects use different encryption systems to generate different system performance on different smartphones. It would not be reasonable to compare these operations solely by means of performance, since there are at least four elements engaged: the information encoding technique, a smartphone camera and, ultimately, the emiter characteristics, light propagation, i.e. sight line (LOS) or non-sicht line (NLOS). The following facts illustrate these distinctions. Works [68] applied distinct approaches and were able to produce comparable throughput values with distinct camera capacities, such as a roll or a global shutter respectively. In addition, Schmid et al. [106] and Ferrandiz-Lahuerta et al. [36] receive two magnitude commands greater than [103] and [68] but depend on the propagation of non-line-of-sight (NLOS). We introduce a taxonomy to assist in classifying the past field research.

2.4.1 Line of Sight Communications

CamCom[102] utilizes UFSOOK to encode information at frame rate harmonics and decode information by processing aliased sub-sampled frequencies. The main benefit of this system is that it operates with both worldwide and rolling shutter sensors. Note that the IEE 802.15.7 m standard was supplied by UFSOOK. It operates at about 120Hz frequencies and can cause fluttering. Luxapose, a VLC indoor positioning method with the accuracy of a decimeter, has been presented by authors in [66]. The system is composed of a camera sensor that captures various LED luminaires placed on the roof and uses a distinctive blink frequency to identify the device. The mobile device then translates the LED identifiers in position coordinates that can be used by selection of a cloudlet through triangulation. The authors used OpenCV library library software visualization [63] for an LED detection and frequency detecting method: they transformed the image to black, blurred it, and used the Otsu binary filter [92] to detect each blob's contours. The frequency estimation of each ROI is conducted by the YIN algorithm, after each area of interest (ROI), namely each sender, is found [24]. The average time of smartphone processing for the 33 MP pictures is around 9: picture taking 4.46 s, uploading 3.41 s, image processing 0.3 s, estimated location (0.87 s). The experimental assessment has shown that LiTell offers less than 3 ° error meter precision and orientation. By using the compact PD sensor board connected to a smartphone, Pulsar [41] is LiTell expanding. It utilizes PD to better discriminate against present, fluorescent or

conventional, ceiling lamps by its intrinsic optical emission properties. It also overcomes the photodiode lack of space resolution with the front camera smartphone. Pulsar thus determines the photogrammetry angle of entry of the source of light to triangulate the 3D position and even the equipment's orientation. When unmodified lED / FL lighting, i.e. color and geometric format, is used by iLamp to identify the lamp as the landline using a smartphone camera. In the 3D location ILAMP is also introduced, using the sensor-assisted photogram metry method, with a 3.5 cm (2.8 °) tiny 90-percentile mistake. The authors are using iLamps on their Android phone, and tariff cycling reduces energy usage and latency. The experimental assessment shows that the system is low latency, ranging from 400 to 700 m that is less than one and a half, opposed to the Luxapose or LiTell. HU et al. offers a scheme in ColorBars [56] which uses RGB LEDs to enhance the communication between the LED and the camera. This is how ColorBars works. The information flow is split into blocks of bits on the transmission hand, and error correction coding is used for each block. To handle data loss owing to IFG and ISI mistakes, ColorBars utilizes RS coding. Data blocks and parity bits are used to form packets, where each packet includes the header and packet delimiter. The encoded bits of the packages are then modulated by CSK modulation to form a stream of symbols: The bits are divided into three bits, and each block is mapped to a CSK-compatible color symbol. The devoted lighting symbols of white light are placed to always maintain perceived colors the same. In addition, ColorBars emitters regularly send calibration packets to face the color variety on their smartphones. The symbols in the calibration packets are used for demodulating symbols as reference symbols in the data packets. As in the case of Lahuerta et al.[36], the authors determine packet sizes that fit into the IFG's picture as broadly as possible. The disadvantage of this strategy is that it must be constant, small enough to cover the entire image between the receiver and the emitter. ColorBars utilizes the CIELab color space to demodulate on the recipient side. CIELab consists of three color channels with one lightness channel L and two color channels (a and b). In the test bed and experimental assessment, the writers carried out ColorBars demonstrated that the data rate for iPhone 5S systems could be 5.2kbit / s on Nexus 5, and 2.5 kbit / s. RollingLight authors [68] researched the rolling shuttle impact widely and felt that the idle time gap between two successive frameworks is unpredictable and variable. This idle gap causes the data packets to be lost in the captured image as shown in Figure 2.3. In the case of a frame period slightly longer than the packet duration this packet loss was observed. Therefore one

picture can capture the maximum packet, but without a complete packet, the variable idle range can lead to a random loss of packets and frames. RollingLight adds an xor parity symbol to both packets in order to tackle this issue. If either of the two symbols is lost, the remaining one with the parity symbol can be retrieved via XOR gate. Hao et al. lately introduced CeilingCast [48]. More lately. Their VLC system uses CDs to generate a LOS broadcast channel with a smart phone, using commercial off-shel (COTS) LED streaks. Innovative systems for both encoding and decoding have been suggested using the mixture of OOK and Manchester coding in [22] to enhance the accuracy and performance of the linking. They use the Raptor Code without rates to confront both the camera and the distance caused the unavoidable packet erasureIn order to make the Luby Transform Code more efficient, a proposal was made to use the internal and external code to improve its efficiency: first of all, the original packs are used to derive a series of intermediate packs, so that the intermediate packets are able to rebuild the original paquets. The repair packages are then produced using LT encoding. Each intermediate packet comes from the XOR door. Encoded final packages are the mix of the original and the repair packages. As for LT code, the downside is the surface charge for the k extra packs and the addition of information to each of those packs in order for the receiver to correctly reconstruct the initial signal. Since CeilingCast depends on the entire lighting scheme, it can leverage various LED lines to communicate with MIMO. Before encoding them by means of Raptor Codes, the scheme assigns n packets to each emitter. Thus, by the receiver, one of its n + k packets from any emitter would effectively re-construct the signal. The tests show that CeilingCast reaches 0.4kbit / s with a range of 2,2 m and can produce 1,35 kbit / s per single LED. With 3 LEDs. Intervals of up to 5 m can be shown by the writers. Hesselmann et al. [51] proposed a method to enable two-way camera-smartphone communication. High and tiny pieces are displayed in a certain timeframe by turning on and off smartphone flashs. NRZ OOK modulation with a pulse length of 50 ms is used in the PHY layer. In addition, the authors didn't introduce high-level error detection or framing protocols. Thus, the symbol rate is lower that the camera's frame rate and therefore it is simple to demodulate, without losing the signals at the top of the table. They have implemented a test on a non-root Nexus One to evaluate the flash-based communication's efficiency. It has shown that a maximum production of about 20 bps can be achieved.

2.4.2 Non Line of Sight Communications

NLOS LED-by-cama communications use a lighted surface, i.e. a reflected light, to suppress the necessity to direct the telephone towards an LED as a source of data instead of a direct lens. NLOS LED-to-camera communication generally performs better as the entire image takes the light signal. However, owing to diffuse reflection, which improves the demodulation error, RSS on a NLOS link is considerably diminished. Instead of LOS light propogations, the following work depends on NLOS. Ferrandiz-Lahuerta et al. [36], in contrast to CeilingCast, exploites a light reflection on a wall carefully instead of the LED light. In these circumstances, the rolling shutter model, which encodes information, covers the entire images. Therefore, it is not necessary to detect the emitter and to remove the ROI. The contributions of [36] are two-fold with regard to the seminal Danakis et al. [22] operate with OOK modulation and Manchester coding. The authors first plunged into the Android Camera2 API in November 2014 [43]. They also given a glimpse of the Android setup which lets you look at a shutter object with a smaller definition than the old API camera. This improved the transmitter frequency compared to earlier apps. Secondly, the authors proposed the LED-camera communications protocol and error detection, as well as correction schemes. CRC codes are error detection and correction. The input-bit stream is divided into 24 bits and one CRC4 is calculated for each group. The set of 24 CRCs will be inserted at the end of the bitstream to be sent. A block is then constructed by adding a sequence amount of 7 bits and a group synchronization bit. Every block is then sent twice to verify that each image includes a minimum of one block and 2 blocks in consecutive images. This structure nonetheless assumes that communication is ongoing, without loss, so that the transmission failure is due to lack just one block. In [99], BFS K is used for the introduction of the asynchronous protocol between a LED and iPad. They were designed for a prototype that could connect simultaneously to CMOS cameras on 29 channels with a data rate of ten bps. But demodulation was not carried out in real time on a smartphone, but a laptop app from Matlab was provided. Their technology uses a 1-D Fourier transformation to identify preamble and frequency. Their slide windows are used. If the main focus of their job is the communication channel, they also suggest locating equipment by merely choosing the closest point with the largest RSSI. Recently Yang and others have been proposing to enhance NLOS VLC system efficiency using GSK modulation using ReflexCode. In essence, ReflexCode codes data through superimposition of light emissions from various transmissions and

the clever transformation of damaging interferences. The 4-GSK modulation is obtained from the superposed ONOFF status of three synchronized LED luminaries: a) all three OFF00 (S0), b) the Center ON and S1 for ten (S2) and d) all ON for S3 transmitters, respectively. The receiver hand decoding procedure combines traditional amplitude demodulation with path detection to decode modulated signals on a gray scale and dynamically sets decoding threshrights based on the space symbol distribution. In order to prevent splitting by individual transmitters, the author also designs DC-balanced code. They dealt, as in [48], with demodulation mistakes and intra-frame packet losses. ReflexCode assessment shows that a throughput of up to 3.2 kbit / s can be achieved at a range of 3 m.

In [29] the writers suggest to improve the Network data rate in an NLOS situation a fresh model and design protocols for the link layer. Its protocol, MARTIAN, enables interaction between a smartphone group and smartphone cameras from the light reflection on a wall or image. MARTIAN utilizes Manchester coding on the physical layer together with light intensity modulation. As the intensity of the light greatly depends on the range or angle between the surface and the camera, MARTIAN takes advantage of the intensity variation pattern rather than the absolute intensity value. In 4 light intensity changes 00, 01, 10, 11, for example: 0% to 50%; 0% to 75%; 50% to 75%; and 75% to 75%; 0% to 50% to 05%; and 0% to 80% to 05% to 50%. For example, the smallest amount of intensity is the lowest. In the Link layer, the writers use Fountain Code [81] in order to manage an IFG to split the initial signal into submessages. Du et al [29] suggest to reduce its overhead distribution by implementing a Fountain Code Table, which enables us to use only a couple of bits for maintaining the index of the encoding and considerably increases the achievable information rate, to handle the overheads implemented by the Fountain Code in light camera interaction. Even with an NLOS connection, MARTIAN can reach a data rate of about 1.6 kbit / s. In LiShield, Zhu et al. [42] use the rolling shutter to guard against photography by lighting the physical scene with intelligent LEDs modulated through FSK modulation. This includes any image taken with a dark, vertical CMOS camera. They have also intended systems to unblock approved cameras: a Smartphone completely sync with the transmitter adapts its time to track the emitter frequency hops by means of a particular frequency hopping pattern, which deletes the rolling shutter artifact.

3. WDM BASED VISIBLE LIGHT COMMUNICATION

3.1 WHITE LIGHT-EMITTING DIODES (LED)

LEDs are semiconductor units that provide light if the direction of p-n junction is oriented forward. In addition to traditional lighting sources, LEDs have several benefits, including reduced energy consumption, longer lifetime, increased robustness and smaller sizes. One interesting feature of LEDs is that they are able to switch on and off more quickly than people can tell. By changing the driving current applied to the device, the LED's light energy can be easily modulated. Thus, in addition to becoming popular for lighting reasons, LEDs can also be used for wireless data transmission. LED for architectural lights are also used for the intrinsic diming and color rendering facility. LEDs are used extensively in automotive apps for tail, brake and indicator lamps. Traffic signals also use LEDs to ensure reliability and durability. In white-light generation with LEDs there are generally two ways. In the first place, for example, light can be combined from red, green, and blue (RGB) LEDs. Triple system consists generally of a single package with three emission controls and mixed optics and is often used where different color emissions are required. This system appeals to the VLC as it provides for the transmission of separate data on each LED. The second method is to use a single blue LED that is covered or sometimes embedded in a phosphate capacities that emit redshifted light when absorbing a section of blue light emitted by the LED. Added to the blue component that is not absorbed for the required white color, is the red shifted emission mixed. At present, the subsequent technique is often endorsed due to decreased complexity and costs. However, the rate of complete optical reactions in single chip devices is generally limited by phosphorus. The disadvantageous small modulation index can be enhanced from 3 to 20 MHz if only the blue part of the emitted spectrum is identified.

3.2 SEMICONDUCTOR LASERS

Laser is an acronym for light amplification by stimulated emissions of radiation. Extension (or increase) is done through a quantum mechanical technique which allows the photon, where the energy difference between the two states is photon energy, to boost excitement from higher to

decreased energy levels of an excited electron. The stimulating photon is emitted with the same frequency, stage and direction when the electron is defecated. An optical feedback is required (though not shown in the acronym), usually by inserting the recovery material in the optical resonator of the semi-transparent mirror (or optical cavity). The laser happens if enough energy comes from the gain medium in the cavity.

In order to achieve enduring outcomes, two criteria must be met. The sufficient profit should compensate for all optical losses in the cavity (internal and reflective losses) and repair the field phase following a round tour. The material threshold gain needed to start durable is shown by

$$g_{th} = \frac{1}{\tau}[\alpha_i + \alpha_m] = \frac{1}{\tau}[\alpha_i + \frac{1}{2L}\ln(\frac{1}{R_1 R_2})] \quad (3.1)$$

Where αi and αm are the internal and reflective losses, L the cavity length; and where= value of α= value of Va / Vp is the optical confinement factor (i.e. overlap between active region and optical field, where Va is the active region's volume, and Vp is lasing mode volume), The gain is obtained in a laser with semiconductor by the transition from the lead belt state to the valve band. In this case, the bandgap energy determines the wavelength (or color) of the output light. Typically an intrinsic region sandwiched between p-and n-doped material with a greater band gap than the inherent active substance containing carriers in the active region of a semiconductor laser is the active region. They collect by injecting carriers (electrons and trousers) in the active region. The present threshold Ith is called the injected current required to achieve the target profit (3.4).

The phase condition on the other hand is given by

$$\exp\left(-j\frac{2\pi}{\lambda_0/n_{eff}}.2L\right) = 1 \rightarrow \lambda_0 = \frac{2Ln_{eff}}{m} \quad (3.2)$$

where λ0 is the lasing wavelength (in vacuum), n_{eff} is the effective refractive index of the cavity, and m is an integer number. The Fabry-Perot laser, the edge-emitting laser, is the easiest semiconductor laser possible. The reflections at the split facets offer enough feedback to accomplish lasting together with a large increase over a comparatively lengthy range along the cavity owing to the elevated refractive index between the half-conductor material and air.

3.2.1 Mirror Reflectivity and Gain

The VCSEL is a laser with semi-conductors that, in comparison to edge emitters, orients the visual cavity perpendicular to its semiconductor surfaces. This implies that light from the top layer can be transmitted, which allows easy wafers to test equipment. However, given the vertical cavity, the duration over which photons can communicate with the medium of gain (tenses of nanometres) is very brief, which results in a tiny round trip gain. The reflectivity of both mirrors that define the cavity is extremely high (> 99%) so as to guarantee small optical losses in the cavity. In the Figure there is a schematic cross section and a VCSEL top figure. 3.4. Using distributed Bragg reflectors (DBRs) is usually required for reflectivity. The DBR comprises of a series of pairs with distinct refractive index of alternating μ/4 thick layers. DBRs are typically epitaxial semiconductors or consist of dielectric materials for VCSELs. The amount of pairs required for reflectivity of > 99 percent relies on the refractive layer comparison. The materials available for epitaxial DBRs have a relative low contraction of the refractive indices, requiring a adequate reflectivity of every 20-30 DBR pairs, while dielectric materials offer a far greater contrast in the refractive index and typically require fewer than 10 DBR pairs.

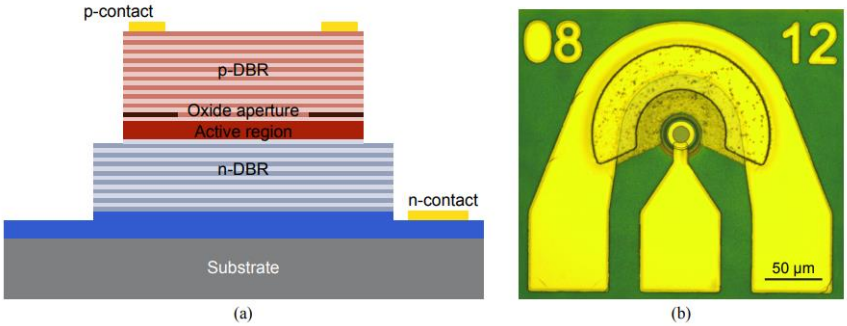

Figure 3.1: (a) Schematic cross-section of a VCSEL, and (b) microscope top view of a VCSEL on chip.

In addition, numerous quantum wells (QBs) within a distinct heterocontainment construction (SCH), where electrons are trapped, leading to a elevated carrier density, form the inherent portion of the active region. In the past, 850 nm VCSELs use GaAs, but with strained In GaAs QWs the differential gain is increased, which is advantageous to achieve a greater velocity.

3.2.2 Transverse Confinement

The photons are vertically restricted by the two DBRs to the active region, however they both must be restricted to the middle and the photons. Examples are etched air bills, implantation of ions, buried tunnel crossing (BTJ), and the oxide opening as demonstrated in Fig. 3.4. The graded air post is clearly the easiest alternative whereby a big refractive contrast index between the semiconductor and the air is limited to the optical field but diffraction and the recombination between carriers and semiconductors cause issues. For the first commercial VCSELs, the aperture was successfully defined by implanting ions, usually protons (Fig. 3.5b). The implanted areas are extremely resistant and confined to the center. The implantation, however, does not alter considerably the refractive indicator, which reduces the optical champ by gaining guidance and thermal lens (due to the increase in the temperature of the actively operating region, which changes slightly the refractive index), which will cause the modal conduct to rely upon the current of injection. The BTJ (Fig. 3.5c) offers both optical and electric containment and has been effectively applied for long wavelength InP-based VCSELs, although InGaAs-based BTJ VCSELs at 1.100 nm have been demonstrated. Although they are hard to perform in shorter wavelengths. Oxide-confined GaAs-based VCSELs, (Fig. 3.5d), are using the selective oxidation of high algaes layers for the forming of oxide apertures, which are both electrical and optical, because the resulting oxide is isolated and has a less refractive index than the non-oxidized material, in contrast to InP-based VCSELs which lack a high quality oxide.

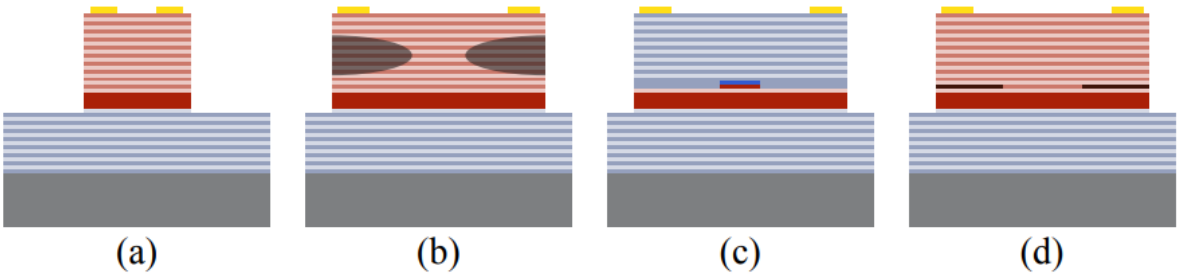

Figure 3.2: Transverse confinement schemes: (a) etched air post, (b) ion implantation, (c) buried tunnel junction, and (d) oxide aperture.

3.2.3 Temperature Effects

The emissions wavelength is fixed by the cavity resonance rather than by its gain peak, since the VCSEL cavity is brief (on order of wavelength) Therefore the emission wavelength shifts red and raises the temperature with current owing to resistive heating of the Joule because the refractive index of the fabric is dependent on temperature. This lead to an increase in GaAs resonant wave length of the VCSELs of 0.06–0.09 nm/ ° C, whereas bandgap deterioration caused an increase in the cavity resonance of the VCSALs of 0.32–0.33 nm/ ° C. The obvious best scenario is when the cavity resonance is aligned with the cavity maximum, which produces the smallest present limit, but the various red-shift rate will place the cavity resonance too far away and increase the present limit to be lasting too much. The cavity resonance is often detonated in relation to the gain peak to allow operation at high temperatures, i.e. the cavity resonance is red-shifted in relation to the gain point at room temperature and the gain is thus aligned at elevate temperature. It was used for working well above 100oC. This method was used.

3.3 HIGH-SPEED MEASUREMENTS

Both tiny and large signal measurements must be conducted in order to characterize the high-speed VCSELs. The tiny reaction to signal modulation offers information to fit the theory transmission function, whereas the major signal tests are nearer to the actual implementation of data transmission.

3.3.1 Small Signal Modulation Response

A vector network analyser (VNA) linked to the VCSEL is used for measuring the tiny signal modulation reaction (S21) by using a bias-T to permit the DC biosections. The VCSEL can be tested straight at the wafer by using VCSEL bond pads that match the soil signal soil (GSG) pitch. A brief multimode fiber connects the output light from the VCSEL, either with an anti-reflecting covered lens package, or by using a bare fiber tip combined. The fiber can be linked to a high-speed photodetector linked to the VNA using a variable optical attenuator (VOA). The VOA is

used to prevent the detector from being saturated. Before the transmission function is adapted to the reaction, the measured information are then corrected for the sample and detector. The fit can be obtained from K-and D-factors. Figure 3.13 shows a schematic of the measuring set-up.

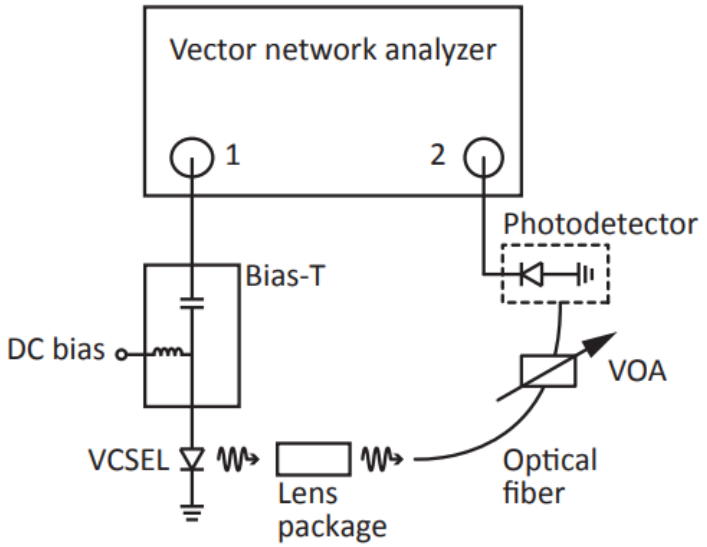

Figure 3.3: Measurement setup for the small signal modulation response.

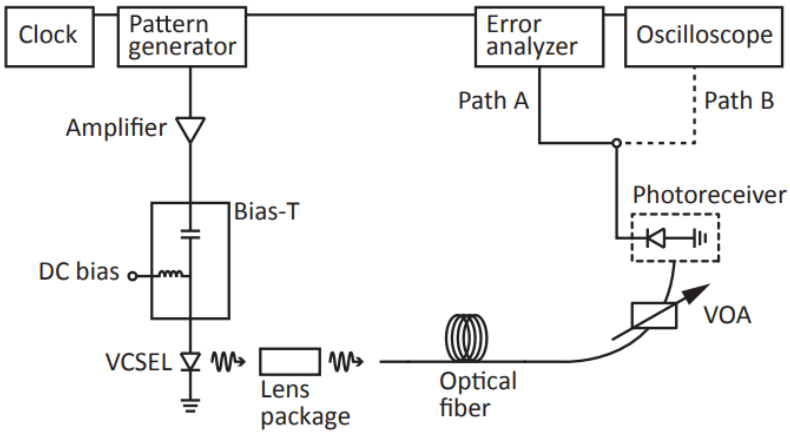

Figure 3.4: Large signal data transmission setup. Path A is used to measure BERs, while path B is used to record eye diagrams.

3.3.2 Large Signal Data Transmission

The modulation in the easiest format is depicted by the on-and off-state environment of the VCSEL. This format is called the "off-key" (OOK) binary modulation. An OOK signal composed of a PRBS (Pseudo Random Bit Sequences) from a pattern generator is amplified and fed to the VCSEL via a bias-T and a GSG probe to conduct large-scale signal transmission experiments. The light is linked by a VOA to a picture recipient by a Multimode fiber. The picture receiver's electric signal is linked to an OSC (an overlay on a signal shape) or the Pattern Generating System to record the amount of mistakes in the received signal. The Pattern Sensor is synchronized with the Pattern Generator. A configuration pattern is displayed in Fig. 4.32. The Bit error rate (BER) can be calculated by calculating the amount of mistakes with the complete amount of bits. The time required to collect mistakes is very long for very small BERs. Therefore, statistical methods need to be used for sensible measurement times. It is required that N_{bits} is detected without any error to ensure a BER below p with a statistical confidence c, where N_{bits} is given by

$$N_{bits} = -\frac{\ln(1-c)}{p} \tag{3.3}$$

A standard requirement is to maintain statistical trust of 95%, which requires a measurement times of 3· 1012, which equals measurement times of 5 and 1 at 10 Gb / s and 50 Gb / s at a rate below 10−12 (sometimes defaults). However, in the work 6· 1012 bits without error were required, which corresponded to a BER lower than 5· 10−13 with 95% trust or, alternatively, a BER lower than 10−12 with 99.75% trust.

3.4 VISIBLE LIGHT COMMUNICATION

Figure 3.1 shows a block diagram of the easy VLC physical layer. The PHY is composed primarily of digital and analog transmitters and also of digital and analog recipients. The transmitter consists of the information source, the database modulator and the DAC. Similarly, an analog to digital (ADC) converter, a baseband demodulator, and a data sink are included in the digital receiber. The analog transmitter involves a LED driving circuit (TCA) and a visible light source, i.e. The LED. LED. The receptor includes a photo-optical, photo-diode, TIA and a band-pass filter. The digital PHY supplies an AC baseband (UAC) signal to a drive system that amplifies the AC signal linearly

and turns it into a stream. Then, by means of a bias tee, this current is added to the DC bias present. The absolute driving current (DC+AC) has to be bigger than zero, given that LEDs work in a linear area with unipolar driving currents. The complete ILED current is transmitted to the LED and the optical Popt is modulated. The received energy (Popt) is targeted to an optical concentration (lens) and transformed into a present IPD in a photoslide through an optical filter. The present AC element is then enhanced by the UPD and filtered by the band-pass (UPD, filter). The band pass filter output is transformed by ADC to a digital signal. Finally, it demodulates the digital signal.

3.4.1 VLC Components

3.4.1.1 OSTAR lighting

OSTAR lighting modules were selected for this project with the aim of illuminating the OMEGA displays area (13 m2 footprint) with a handy amount of LEDs, because they offer significantly better luminance flow than similar high-performance LED lighting systems[4, 3]. With a focus on lighting, for instance room lighting, architectural lighting, industrial lighting, radiator and spot lighting, and flashlights, OSTAR Lighting source was created. Overall, there are four OSTAR Lighting variations which only vary slightly. The first two are based on a module consisting of four semiconductor chips (E2), one without a lens and the other with the lens (ExA and ExB). The remaining two modules are built from a 6 semiconductor chip building (E3). The OSTAR version of the 6 chip is chosen in order to keep the overall number of LEDs low. E3A [3], in French. The technical parameter of OSTAR modules with 6 chips is shown in Table 3.1.

Table 3.1: Electro-optical specifications of OSTAR E3A [9]

OSTAR Type	**E3A**
No. of LED chips	6
Typical bias voltage (V)	21
Corresponding typical bias current (A)	0.7
Corresponding luminous flux (lm) at 0.7 driving current	300
Corresponding typical illuminance (cd)	95
Maximum Dc bias current (mA)	1
Full viewing angle at half illuminance	130^{o}

Figure 3.5: Different types of OSTAR Lightings.

3.4.1.2 DC driving circuit

The typical LED driver circuit is illustrated in Figure 3.6. By changing the driving current applied to the device, the energy of the LED light can be easily modeled. Typical DC driving currents for small packages of LED are 10 mA and driving currents can be greater than 1 A for lighting white LEDs. It was assessed that excess heat dissipation from the LED affected the standard optical power of the LED driving current beyond 900 mA, and these values were therefore lowered when information were adapted. Commercial driver ICs and units supply the driving current of several hundred milliamps at multiple volts of OSTAR. In the kHz or MHz region these instruments generate electric noise typically. This noise does not influence the objective of lighting as it is an issue in communication with information. However, the exposure to interference of the transmitted data signal reduces this electrical noise from the DC source. In this situation, the use of spectrally efficient modulation increases the information rates beyond the bandwidth limit.

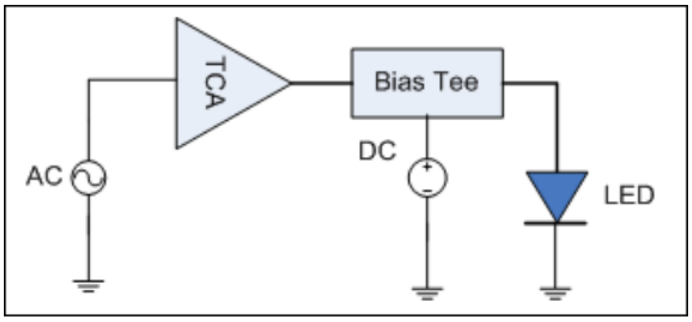

Figure 3.6: Typical LED driver circuit for modulating the optical output form (white LED) [16]

3.4.2 Modulation

Different plans were examined. NRZ-OOK is used for several demonstrations and it benefits from simplification and excellent immunity to LED non-linearity. NRZ-OOOK is a non-return on-off-keying system. The SNR, which makes multilevel modulation appealing, has been studied for this purpose, and discrete multitoned (DMT). The bandwidth of the transmitter side of OMEGA is limited to 10 MHz in the data link project. The obstacle for the target data rate of OMEGA of 100 Mbit / s is this. For example, spatial multiplexing equalization and multi-level modulation can overcome this bandwidth restriction. The OMEGA VLC prototype is based on either this latter one or combined with multi-level equalization modulation. VLC information transfer over 100 Mbit / s has been proved for a 3-dB bandwidth of ± 20 MHz by Grubor et al. This results were obtained using the modulation of quadrature amplitude with discrete multi-tone.

3.5 WAVELENGTH MULTIPLEXING DIVISION (WDM)

We launched the multiplexing system (WDM) for wavelength division and the PDM concept. The following nonlinear CNLS equations:

$$\frac{\partial A_x}{\partial z} + b' \frac{\partial A_x}{\partial t} - \frac{i}{2} \beta_2 \frac{\partial^2 A_x}{\partial t^2} + i a_0 \left(|A_x|^2 + \frac{2}{3} |A_x|^2 \right) A_x = 0 \qquad (3.4)$$

$$\frac{\partial A_y}{\partial z} - b' \frac{\partial A_y}{\partial t} - \frac{i}{2} \beta_2 \frac{\partial^2 A_y}{\partial t^2} + i a_0 \left(|A_y|^2 + \frac{2}{3} |A_y|^2 \right) A_y = 0 \quad (3.5)$$

Ax(z, t) and Ay(z, t) are represented by complex x-and y-polarized signals in the equations (3.0a) and (3.0b), at distances z and in the time t delayed. The ground step is assumed to maintain polarization and the group delay is represented by β1x and β1y per unit length, and b′ is (β1x-β1y)/2 rescaled to achieve the right dispersion mode (PMD) statistics for polarization. The CD fiber is modeled by β1x= β2y= β2. The dispersed fibers. Ax and Ay are absorbed by the fiber attenuation. The Fourier (SSSF) technique is used in the vector simulations for each phase of simulation. The simulated optical vector field is dispersed over the Poincaré sphere after each rough move.

With the x-polarized field, we have a $A_x(z,t) = \sum_{n=1}^{N} d_n a(t - T_{sym})$ total to(t-T sym) functions in single-channel systems when not using its special direction. If N is the number of symbols in simulation, dn is the nth data symbol, a(t) is the pulse shaping function and Tsym is the time interval of the symbol. In single channel systems system bandwidth is roughly inversely proportional to Tsym.

Ax(z, t) is a complete signal field, which is overlaid with various WDM channels for WDM devices. If five channels are included as our channel of concern in the simulation with the center channel, we have

$$A_x(z,t) = \sum_{m=-2}^{2} \sum_{n=1}^{N} d_n^m a(t - nT_{sym}) \exp(j2\pi m F_{wdm} t) \quad (3.6)$$

The d_n^m U is the n^{th} information sign on the m^{th} of the wavelength channel where F_{wdm} is the channel spacing. Approximately (M-1) F_{wdm} is system bandwidth. Where M is the complete channel number. Given that F_{wdm} is often far bigger than $1/T_{sym}$, there is a much wider bandwidth than a single channel signal for the complete range of WDM signals. Depending on how these wavelength can interfere, small spikes in the time domain are generated and the WDM devices are subject to greater dispersion or walking off impacts. Note that in (3.1), m= −2, −1, 0, 1, and 2 are denoting the five wavelength channel numbers.

Here we use the following analytical formula to select the simulation step-size h(z) for the coarse step,

$$\gamma P_{max}(z)h(z)(D\Delta\lambda\Delta f h(z))^2 = \Delta\xi \quad (3.7)$$

In (3.2), D is the parameter of the fiber dispersion, "so" or "soft" means the bandwidth of a signal, $P_{max}(z)$ refers to the optical maximum energy of the simulate wave form at z. B. The step-size h is entered as h(z) because h is z dependent. Parameter β is referred to as the bound of a local error and constitutes an error in pulsed width because of a final h [11]. Note: for WDM schemes, the complete field bandwidth is to be used in −μ or − in (3.2); for simulations with a wide range of channels, the value of −f is about equivalent to the amount of channels multiplying channel spacing. In (3.2), Pmax(z), which must be changed as follows for PM signals, is the only parameter to be calculated during the simulation run.

$$P_{max}(z) = max_t(|A_x(z,t)|^2 + |A_y(z,t)|^2) \quad (3.8)$$

If you study a certain channel, e.g. the center channel or an edge channel, you need to filter out the complete field to achieve the GE-calculation signal of interest. The RÅO for PM-QPSK scheme with consistent detection is altered in vector areas,

$$nsd(L) = \sqrt{\frac{\int(|A_x(L,t)-A_{xt}(L,t)|^2+|A_y(L,t)-A_{yt}(L,t)|^2)dt}{\int(|A_{xin}(0,t)-A_{yin}(0,t)|^2)dt}} \quad (3.9)$$

In the cases where $A_x(L, t)$ and $A_y(L, t)$ represent an approximate simulated Waveforms at distance L, $A_{xt}(L, t)$, andAyt(L, t), the inputs are $A_{xin}(L, t)$ and $A_{yin}(L, t)$. Equation has to be modified to portray the phase LE of (z, z+h(z)): modifications in l to z+h(z), modifications in A_x and A_y to the approximately saved solution at z+h(z), and the approximate saved solution at and for simulation over (z, z+h (z)) is provided to A_x and A_{yt}.

4. IMPLEMENTATION AND RESULTS

The multiplexing division of wavelength is a technique for simultaneously transmitting more than one data stream on one channel. This divides the whole canal into distinct slots by wavelength and assigns a distinct wavelength slot to each signal source. The information streams are identified and forwarded to each destination simultaneously on the same channel on the receiver side. The channel has a range of 400 to 750 nm in the VLC scheme, i.e. an optical domain. Varying color sources can generate light from distinct wave lengths. The wavelengths of each color. If you look at white light, you can achieve the objective of indoor lighting and communication. The red, green, and blue LEDs produce low quality white light but increase channel use with the blend of red, orange, yellow, green, purple, white and indigo. The spectral range of the LED is big, so that the channels do not communicate with the sign (ISI) the distinction between them must be maintained. But if pointing lasers with a very low spectral thickness and a canal spacing of 1–2 nm are used, it is possible to split the channel into more slots and simultaneously transfer a greater amount of information streams. This is known as the thick multiplexing wavelength (DWDM) division. This increases the information rate also because distinct information signals are simultaneously transmitted and the laser is switched at a greater rate.

4.1 SYSTEM DESIGN

A scheme displayed here in Figure. 4.1 on OptiSystem software is shown. Various signals in the shape of square waves are produced. The eight color LEDs change these signals to modulate light. The intensity modulation method is employed in this specific project, i.e., the output light strength varies based on the input signal amplitude. The output light from these multiple colorful LEDs merge passive optical systems such as lenses with white light. This is called multiplexing or multiplexing of color splitting optical wavelength division. It is transferred in free space by multiplexing signal. The transmission range is restricted and LOS route is needed, but the data rate is very big. In this situation, the scheme for indoor environments is simulated here at a range of 1500 m. Each color light is segregated from the white light of the recipient by distinct color filters. These color filters are optical components which are passive and serve as belt color wavelength

filters. In comparison with the pre-FEC threshold, the transmitted light is then identified and transformed in electricity by the use of different photo detectors for each color signal. The scheme is appropriate because the BER is below the FEC limit.

This system is easy to develop with hardware. Separate data signals guide different color LEDs. Different color and image diodes according to their wavelengths are used for each LED. With the help of high energy LEDs, unique LEDs (resonant cavity linked to LEDs) or LED arrays, distance between the transmitter and the receiver must be reduced. It is necessary to improve the amount of optical energy.

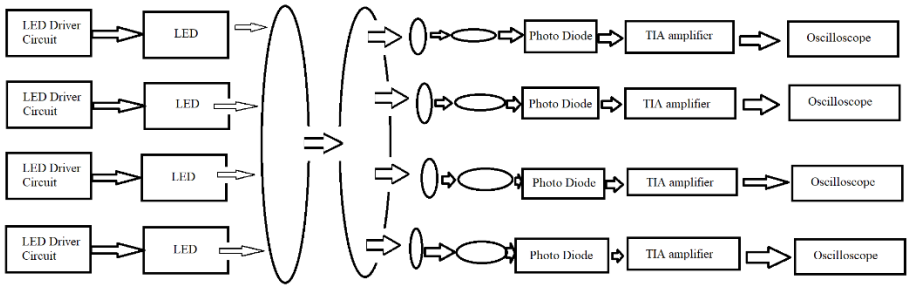

Figure 4.1: 4x1 WDM based VLC

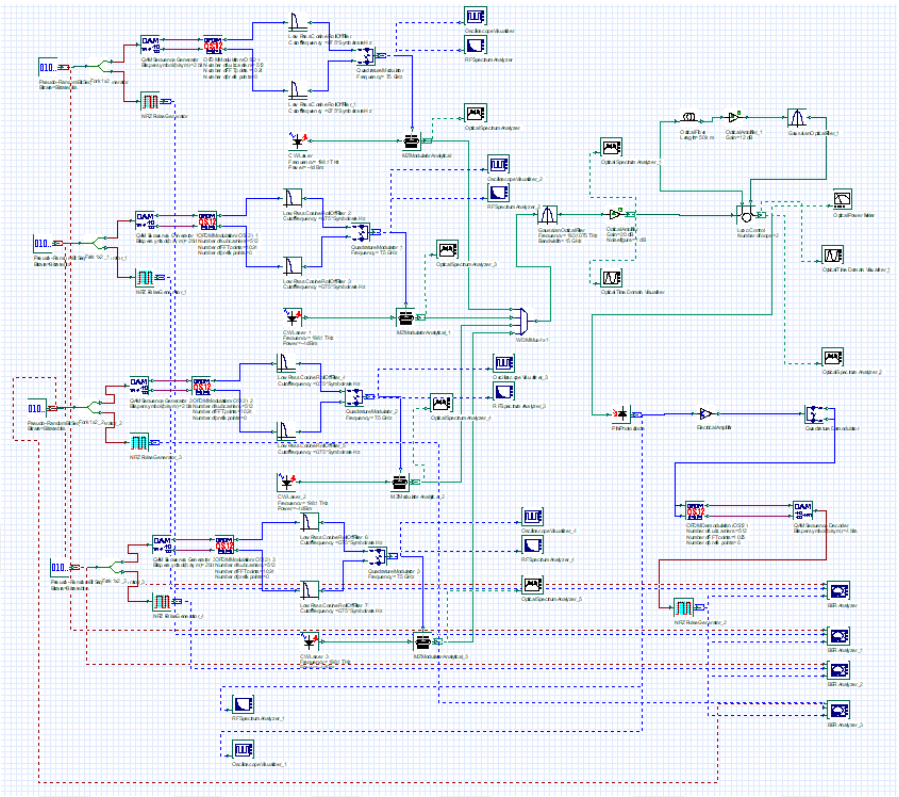

Figure 4.2: 4x1 WDM based VLC structure in Optisystem

This scheme has 100 Mbps with BER below FEC boundaries, i.e. the range from 3, 8 till 10^{-3} for the range between 100 and 1700 m, which can be achieved. As shown below (Figure. 4.2), with all the color wavelengths, the white light range is:

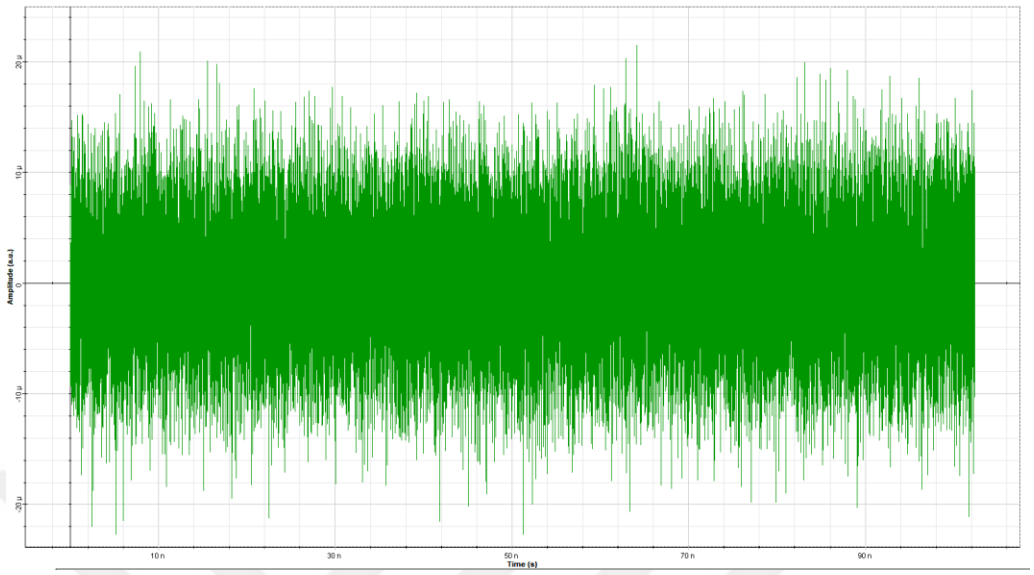

Figure 4.3: Spectrum of white light

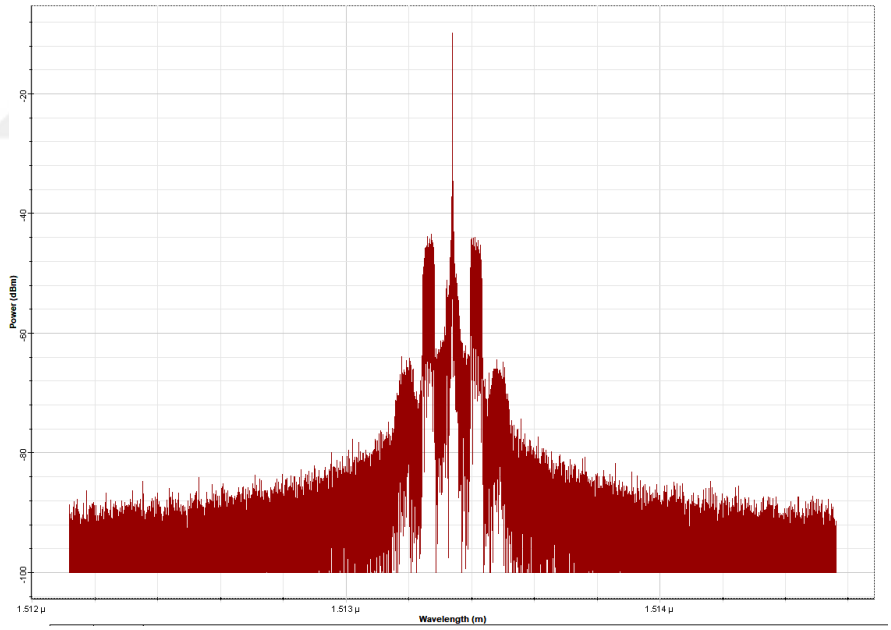

Figure 4.4: Spectrum of light

We applied the system according to the figure that we explained using Optisystem 14 simulator. In this work we had 4 Quadrature Amplitude Modulation based (QAM) based Orthogonal frequency-division multiplexing (OFDM) signal from 100 Mbps pseudo random signal that applied on 4x1 WDM to process the signals into one signal to a 2000 m fiber optical cable. The

output of the 4x1 WDM is connection OFDM demodulator and QAM demodulator and ends with a pulse generator to check the signal characteristics.

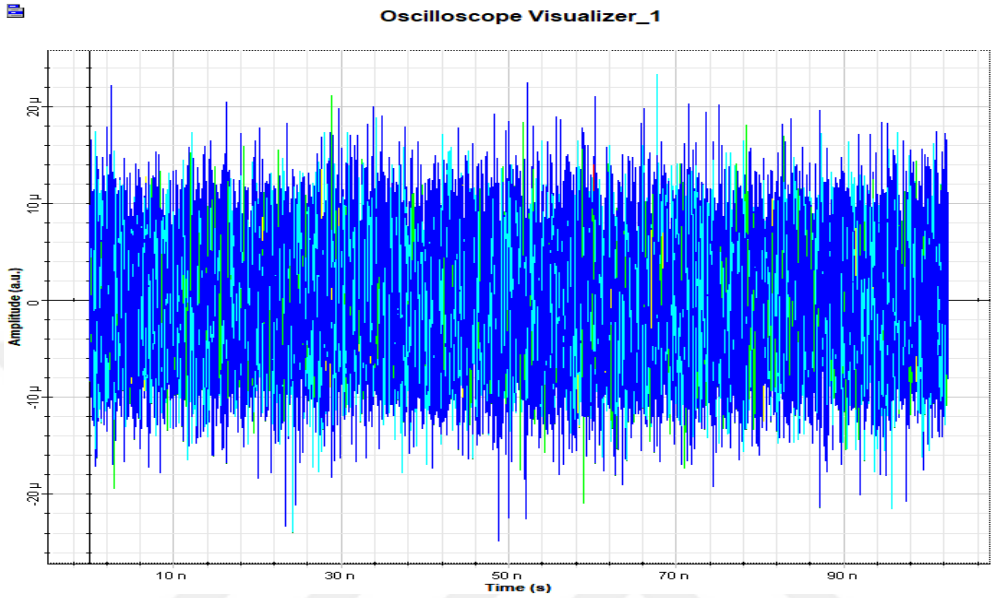

Figure 4.5: The demodulated output signal

5. CONCLUSION

The rate of data of 100 mbps is very low when compared to the limit of previous errors with a maximum bit error rate of $3x10^{-8}$. This scheme is used for 1500 m transmitting range. The LED arrays may increase optical power levels, thus increasing the transmission distance. It can also be improved with pointed laser diodes that provide monochromatic light of high intensity, which also improves the rate of information. By enhancing modulative methods the data rate can also be improved. OFDM with QAM modulation is one of the best methods for VLC. With the 4-QAM OFDM modulation technology, the data rate is 10 Gbps, a further increase can be made with 512 QAM OFDM signal. The WDM can be used to achieve a multiplex of more than 100 Gbps by the greater QAM OFDM signal level.

5.1 SUGGESTIONS

Several avenues of future work can be proposed based on the results of this work. The observation of complex dislocation patterns in the degraded WDM-VLC method suggests that it would be telling if computer code could be developed that would model the patterns that dislocations would create based on controlling parameters such as residual stress fields, non-radiative recombination, and which would take into account the possible effects of the Mullen-Sekerka instability (as discussed in D). In order to compliment the in-situ TEM experiment exploring the effects of current injection on III-V semiconductor degradation behavior, experiments exploring in real-time and on a nanoscale level, the degradation behavior of III-V materials under high optical injection and under the influence of electric fields should be developed. Thus, details of a partially developed optical in-situ experiment are discussed in Appendix G. While the focus of the in-situ studies described in this work has been on sectioned WDM-VLC samples, the residual stress state in a WDM-VLC is complex and cannot be easily determined. Thus, by employing simpler structures in which the stress state can be engineered (i.e. from lattice mismatch), a correlation between the degradation behavior and the stress state can be made.

It is known from the oxide studies described in this thesis that the compositions in the range of $Al_xGa_{1-x}As_yP_{1-y}$ ($y > 0.80$) undergo rapid thermal oxidation in which a volume expansion occurs

(presumably due to the retention of P oxides). Thus additional characterization of these oxides, particularly using a surface oxide geometry, needs to be performed in order to determine that composition for which volume change upon oxidation is minimized. Presumably, a lateral oxide of the composition thus determined can be used as an oxide-confinement layer in a WDM-VLC to minimize the degree of stress induced.

Furthermore, the oxidation of semiconductor materials can be modeled as the summation of the reaction limited (linear) growth and diffusion limited (parabolic) growth contributions to the overall oxide length. It is thus possible to explicitly determine the activation energies of the diffusion and reaction limited processes by first fitting the functional form given in Equation 2-10 to a plot of oxide length versus time for a specific oxidation temperature to extract the parameters kl and kp. The coefficients thus obtained, which contain the activation energy terms, can be plotted using the Arrhenius method for which the measured slopes are equal to the activation energies. This method is demonstrated for the oxidation of Si and for the oxidation of AlAs. Thus, additional characterization of the oxide lengths with time and temperature, especially for the commercially interesting oxide of $Al_xGa_{1-x}As_yP_{1-y}$ (y 0.78) will provide such information.

Finally, further insight into the relative effects of the reactive and diffusive mechanisms on the oxidation of III-V materials may be gained by characterizing chemical profiles in the vicinity of the oxide front. Presumably, for conditions of strong diffusive dependence (i.e. the time required to complete the reaction at the oxidation front is small compared to the time required for the oxidant to reach the front), there will be high chemical gradients across the oxidation front.

REFERENCES

[1] (2018). Metal | Apple Developer Documentation.

[2] (2018). RenderScript | Android Developers.

[3] (2018). Rtone - IOT Makers.

[4] Abedi, A. and Brecht, T. (2016). Examining Relationships Between 802.11n Physical Layer Transmission Feature Combinations. In Proceedings of the 19th ACM International Conference on Modeling, Analysis and Simulation of Wireless and Mobile Systems - MSWiM '16, pages 229–238, New York, New York, USA. ACM Press.

[5] Afgani, M., Haas, H., Elgala, H., and Knipp, D. (2006). Visible light communication using OFDM. In 2nd International Conference on Testbeds and Research Infrastructures for the Development of Networks and Communities, TRIDENTCOM 2006, volume 2006, pages 129–134.

[6] Aldalbahi, A., Rahaim, M., Khreishah, A., Ayyash, M., Ackerman, R.,Basuino, J., Berreta, W., and Little, T. D. (2016). Extending ns3 to simulate visible light communication at network-level. In 2016 23rd International Conference on Telecommunications (ICT), pages 1–6. IEEE.

[7] An, C., Li, T., Tian, Z., Campbell, A. T., and Zhou, X. (2015). Visible Light Knows Who You Are. In Proceedings of the 2nd International Workshop on Visible Light Communications Systems - VLCS '15, pages 39–44, New York, New York, USA. ACM Press.

[8] Armstrong, J. and Lowery, A. (2006). Power efficient optical OFDM. Electronics Letters, 42(6):370–372.

[9] Astudilloy, D., Chaput, E., and Beylot, A.-l. (2014). PRAVDA: Pseudo random network coding in vanet for data download. In 2014 IFIP Wireless Days (WD), pages 1–3. IEEE.

[10] Axis Communications (2011). CCD and CMOS sensor technology. Technical report.

[11] Bahl, P., Padmanabhan, V. N., Bahl, V., and Padmanabhan, V. (2000). Radar: An in-building rf-based user location and tracking system. Institute of Electrical and Electronics Engineers, Inc.

[12] Bakker, A. (2014). Comparing Energy Profilers for Android. 21st Twente Student Conference on IT, 21.

[13] Brouwers, N., Zuniga, M., and Langendoen, K. (2014). NEAT. In Proceedings of the 12th ACM Conference on Embedded Network Sensor Systems - SenSys '14, pages 16–30, New York, New York, USA. ACM Press.

[14] Carroll, A. and Heiser, G. (2010). An analysis of power consumption in a smartphone. Proceedings of the 2010 USENIX conference on USENIX annual technical conference, pages 21–21.

[15] Chau, Y. and Yu, S.-H. (2001). Space modulation on wireless fading channels. IEEE Vehicular Technology Conference, 3(54ND):1668–1671.

[16] Chen, S.-H. and Chow, C.-W. (2014). Color-Shift Keying and CodeDivision Multiple-Access Transmission for RGB-LED Visible Light Communications Using Mobile Phone Camera. IEEE Photonics Journal, 6(6):1–6.

[17] Chi, N., Wang, Y., Wang, Y., Huang, X., and Lu, X. (2014). Ultra-highspeed single red-green-blue light-emitting diode-based visible light communication systemutilizing advanced modulation formats. Chin. Opt. Lett., 12(1):010605.

[18] Chow, C.-W., Chen, C.-Y., and Chen, S.-H. (2015). Enhancement of Signal Performance in LED Visible Light Communications Using Mobile Phone Camera. IEEE Photonics Journal, 7(5):1–7.

[19] Chowdhury, H. and Katz, M. (2014). Cooperative data download on the move in indoor hybrid (radio-optical) WLAN-VLC hotspot coverage. Transactions on Emerging Telecommunications Technologies, 25(6):666–677.

[20] Colvin, A. (1983). CSMA with collision avoidance. Computer Communications, 6(5):227–235.

[21] Corbellini, G., Aksit, K., Schmid, S., Mangold, S., and Gross, T. R. (2014). Connecting networks of toys and smartphones with visible light communication. IEEE Communications Magazine, 52(7):72–78.

[22] Danakis, C., Afgani, M., Povey, G., Underwood, I., and Haas, H. (2012). Using a CMOS camera sensor for visible light communication. 2012 IEEE Globecom Workshops, GC Wkshps 2012, pages 1244–1248.

[23] De Cheveigné, A. and Kawahara, H. (2002). YIN, a fundamental frequency estimator for speech and music. The Journal of the Acoustical Society of America, 111(4):1917–30.

[24] Dehghani Soltani, M., Wu, X., Safari, M., and Haas, H. (2016). Access point selection in Li-Fi cellular networks with arbitrary receiver orientation. In 2016 IEEE 27th Annual International Symposium on Personal, Indoor, and Mobile Radio Communications (PIMRC), pages 1–6. IEEE.

[25] Di Renzo, M., Haas, H., Ghrayeb, A., Sugiura, S., and Hanzo, L. (2014). Spatial Modulation for Generalized MIMO: Challenges, Opportunities, and Implementation. Proceedings of the IEEE, 102(1):56–103.

[26] Dietz, P., Yerazunis, W., and Leigh, D. (2003). Very Low-Cost Sensing and Communication Using Bidirectional LEDs. In UbiComp 2003: Ubiquitous Computing, pages 175–191. Springer Berlin Heidelberg.

[27] Dissanayake, S. and Armstrong, J. (2013). Comparison of ACO-OFDM, DCO-OFDM and ADO-OFDM in IM/DD systems. Journal of Lightwave Technology, 31(7):1063–1072.

[28] Do, T.-h. and Too, M. (2015). Analysis on Visible Light Communication using Rolling Shutter CMOS Sensor. In International Conference on Information and Communication Technology Convergence (ICTC), number 1, pages 755–757. IEEE.

[29] Du, H., Han, J., Jian, X., Jung, T., Bo, C., Wang, Y., and Li, X.-Y. (2017). Martian: Message Broadcast via LED Lights to Heterogeneous Smartphones. IEEE Journal on Selected Areas in Communications, 35(5):1154–1162.

[30] Du, W., Liando, J. C., and Li, M. (2016). SoftLight: Adaptive visible light communication over screen-camera links. In IEEE INFOCOM 2016 – The 35th Annual IEEE International Conference on Computer Communications, pages 1–9. IEEE.

[31] Duque, A., Stanica, R., Rivano, H., and Desportes, A. (2016). Unleashing the power of LED-to-camera communications for IoT devices. In Proceedings of the 3rd Workshop on Visible Light Communication Systems - VLCS '16, pages 55–60, New York, New York, USA. ACM Press.

[32] Elliott, E. O. (1963). Estimates of Error Rates for Codes on Burst-Noise Channels. Bell System Technical Journal, 42(5):1977–1997.

[33] Fan, L., Liu, Q., Jiang, C., Xu, H., Hu, J., Luo, D., He, Z., and Huang, Q. (2016). Visible light communication using the flash light LED of the smart phone as a light source and its application in the access control system. In 2016 IEEE MTT-S International Wireless Symposium (IWS), pages 1–4. IEEE.

[34] Fath, T. and Haas, H. (2013). Performance comparison of mimo techniques for optical wireless communications in indoor environments. IEEE Transactions on Communications, 61(2):733–742.

[35] Fath, T., Haas, H., Di Renzo, M., and Mesleh, R. (2011). Spatial Modulation Applied to Optical Wireless Communications in Indoor LOS Environments. In 2011 IEEE Global Telecommunications Conference – GLOBECOM 2011, pages 1–5. IEEE.

[36] Ferrandiz-Lahuerta, J., Camps-Mur, D., and Paradells-Aspas, J. (2015). A Reliable Asynchronous Protocol for VLC Communications Based on the Rolling Shutter Effect. In 2015 IEEE Global Communications Conference (GLOBECOM), pages 1–6. IEEE.

[37] Fitzek, F., Pedersen, M. V., Heide, J., and M?dard, M. (2010). Network Coding: Applications and Implementations on Mobile Devices. In Proceedings of the 5th ACM

workshop on Performance monitoring and measurement of heterogeneous wireless and wired networks - PM2HW2N '10, page 83, New York, New York, USA. ACM Press.

[38] Galal, M. M., El Aziz, A. A., Fayed, H. A., and Aly, M. H. (2014). Employing smartphones Xenon flashlight for mobile payment. In 2014 IEEE 11th International Multi-Conference on Systems, Signals & Devices (SSD14), pages 1–5. IEEE.

[39] Galal, M. M., Fayed, H. A., Aziz, A. A. E., and Aly, M. H. (2013a). Smartphones for Payments and Withdrawals Utilizing Embedded LED Flashlight for High Speed Data Transmission. In 2013 Fifth International Conference on Computational Intelligence, Communication Systems and Networks, pages 63–66. IEEE.

[40] Galal, M. M., Fayed, H. a., Aziz, A. A. E., Aly, M. H., and El Aziz, A. A. (2013b). Smartphones for Payments and Withdrawals Utilizing Embedded LED Flashlight for High Speed Data Transmission. Computational Intelligence, Communication Systems and Networks (CICSyN), 2013 Fifth International Conference on, pages 63–66.

[41] Galisteo, A., Juara, D., Wang, Q., and Giustiniano, D. (2018). OpenVLC 1.2 : Achieving Higher Throughput in Low-End Visible Light Communication Networks.

[42] Giustiniano, D., Tippenhauer, N. O., and Mangold, S. (2012). Lowcomplexity Visible Light Networking with LED-to-LED communication. In 2012 IFIP Wireless Days, pages 1–8. IEEE.

[43] Google (2018). Android Developers Camera2 API Guide.

[44] Greenan, K. M., Miller, E. L., and Thomas J. E. Schwarz, S. (2008). Optimizing Galois Field Arithmetic for Diverse Processor Architectures and Applications. In 2008 IEEE International Symposium on Modeling, Analysis and Simulation of Computers and Telecommunication Systems, pages 1–10. IEEE.

[45] Grobe, L., Paraskevopoulos, A., Hilt, J., Schulz, D., Lassak, F., Hartlieb, F., Kottke, C., Jungnickel, V., and Langer, K.-D. (2013). High-speed visible light communication systems. IEEE Communications Magazine, 51(12):60–66.

[46] Gu, L. and Stankovic, J. A. (2005). Radio-Triggered Wake-Up for Wireless Sensor Networks. Real-Time Systems, 29(2-3):157–182.

[47] Haas, H., Yin, L., Wang, Y., and Chen, C. (2016). What is LiFi? Journal of Lightwave Technology, 34(6):1533–1544.

[48] Hao, J., Yang, Y., and Luo, J. (2016). CeilingCast: Energy efficient and location-bound broadcast through LED-camera communication. In IEEE INFOCOM 2016 - The 35th Annual IEEE International Conference on Computer Communications, volume 2016-July, pages 1–9. IEEE.

[49] Hao, T., Zhou, R., and Xing, G. (2012). COBRA: color barcode streaming for smartphone systems. Proceedings of the 10th international conference on Mobile systems, applications, and services - MobiSys '12, page 85.

[50] Hernández Marcano, N., Sørensen, C., Cabrera G., J., Wunderlich, S., Lucani, D., and Fitzek, F. (2016). On Goodput and Energy Measurements of Network Coding Schemes in the Raspberry Pi. Electronics, 5(4):66.

[51] Hesselmann, T., Henze, N., and Boll, S. (2010). FlashLight – Optical Communication Between Mobile Phones and Interactive Tabletops. ACM International Conference on Interactive Tabletops and Surfaces, pages 135–138.

[52] Hoque, M. A., Siekkinen, M., Khan, K. N., Xiao, Y., and Tarkoma, S. (2015). Modeling, Profiling, and Debugging the Energy Consumption of Mobile Devices. ACM Computing Surveys, 48(3):1–40.

[53] Hou, J. and O'Brien, D. (2006). Vertical handover decision-making algorithm using fuzzy logic for the integrated radio-and-OW system. IEEE Transactions on Wireless Communications, 5(1):176–185.

[54] Hranilovic, S., Lampe, L., and Hosur, S. (2013). Visible light communications: the road to standardization and commercialization (Part 1) [Guest Editorial]. IEEE Communications Magazine, 51(12):24–25.

[55] Hranilovic, S., Lampe, L., Hosur, S., and Roberts, R. (2014). Visible light communications: the road to standardization and commercialization (Part 2) [Guest Editorial]. IEEE Communications Magazine, 52(7):62–63.

[56] Hu, P., Pathak, P. H., Feng, X., Fu, H., and Mohapatra, P. (2015a). ColorBars. In Proceedings of the 11th ACM Conference on Emerging Networking Experiments and Technologies - CoNEXT '15, pages 1–13, New York, New York, USA. ACM Press.

[57] Hu, P., Pathak, P. H., Feng, X., Fu, H., and Mohapatra, P. (2015b). ColorBars. In Proc. 11th ACM Conf. Emerg. Netw. Exp. Technol. - Conex. '15, pages 1–13, New York, New York, USA. ACM Press.

[58] Hu, W., Gu, H., and Pu, Q. (2013). LightSync. In Proceedings of the 19th annual international conference on Mobile computing & networking - MobiCom '13, page 15, New York, New York, USA. ACM Press.

[59] Hu, W., Mao, J., Huang, Z., Xue, Y., She, J., Bian, K., and Shen, G. (2014). Strata: Layered coding for scalable visual communication. 20th ACM Annual International Conference on Mobile Computing and Networking, MobiCom 2014, pages 79–90.

[60] Huang, Z. and Ji, Y. (2013). Design and demonstration of room division multiplexing-based hybrid VLC network. Chinese Optics Letters, 11(6).

[61] IEEE (2015). IEEE 802.15 WPAN 15.7 Amendment Study Group.

[62] IEEE Computer Society (2011). IEEE Standard for Local and metropolitan area networks - Part 15.7: Short-Range Wireless Optical Communication Using Visible Light. Number September.

[63] Itseez (2015). Open source computer vision library. https://github.com/ itseez/opencv.

[64] Kahn, J. (1997). Wireless infrared communications. Proceedings of the IEEE, 85(2):265–298.

[65] Klaver, L. and Zuniga, M. (2015). Shine: A Step Towards Distributed Multi-Hop Visible Light Communication. In 2015 IEEE 12th International Conference on Mobile Ad Hoc and Sensor Systems, pages 235–243. IEEE.

[66] Kuo, Y.-S., Pannuto, P., Hsiao, K.-J., and Dutta, P. (2014). Luxapose. In Proceedings of the 20th annual international conference on Mobile computing and networking - MobiCom '14, pages 447–458, New York, New York, USA. ACM Press.

[67] Kuo, Y.-S., Verma, S., Schmid, T., and Dutta, P. (2010). Hijacking power and bandwidth from the mobile phone's audio interface. Proceedings of the First ACM Symposium on Computing for Development - ACM DEV '10, page 1.

[68] Lee, H.-Y., Lin, H.-M., Wei, Y.-L., Wu, H.-I., Tsai, H.-M., and Lin, K. C.- J. (2015). RollingLight. In Proceedings of the 13th Annual International Conference on Mobile Systems, Applications, and Services - MobiSys '15, pages 167–180, New York, New York, USA. ACM Press.

[69] Ley-Bosch, C., Medina-Sosa, R., Alonso-González, I., and SánchezRodríguez, D. (2015). Implementing an IEEE802.15.7 Physical Layer Simulation Model with OMNET++. In Distributed Computing and Artificial Intelligence, 12th International Conference, volume 373, pages 251–258. Springer Verlag.

[70] Li, L., Hu, P., Peng, C., Shen, G., and Zhao, F. (2014a). Epsilon: A Visible Light Based Positioning System. 11th USENIX Symposium on Network Systems Design and Implementation, (1):1–13.

[71] Li, T., An, C., Campbell, A., and Zhou, X. (2014b). HiLight. Proceedings of the 1st ACM MobiCom workshop on Visible light communication systems - VLCS '14, pages 45–50.

[72] Li, T., An, C., Xiao, X., Campbell, A. T., and Zhou, X. (2015a). Real-Time Screen-Camera Communication Behind Any Scene. In Proceedings of the 13th Annual International Conference on Mobile Systems, Applications, and Services - MobiSys '15, pages 197–211, New York, New York, USA. ACM Press.

[73] Li, T., Xiong, X., Xie, Y., Hito, G., Yang, X.-D., and Zhou, X. (2017). Reconstructing Hand Poses Using Visible Light. Proceedings of the ACM on Interactive, Mobile, Wearable and Ubiquitous Technologies, 1(3):1–20.

[74] Li, X., Zhang, R., and Hanzo, L. (2015b). Cooperative load balancing in hybrid visible light communications and WiFi. IEEE Transactions on Communications, 63(4):1319–1329.

[75] Liang, K., Chow, C.-W., and Liu, Y. (2016). RGB visible light communication using mobile-phone camera and multi-input multi-output. Optics Express, 24(9):9383.

[76] LiKamWa, R., Ramirez, D., and Holloway, J. (2014). Styrofoam. In Proceedings of the 1st ACM MobiCom workshop on Visible light communication systems - VLCS '14, pages 27–32, New York, New York, USA. ACM Press.

[77] Liu, V., Parks, A., Talla, V., Gollakota, S., Wetherall, D., and Smith, J. (2013). Ambient backscatter: Wireless communication out of thin air. In Computer Communication Review, volume 43, pages 39–50.

[78] Liya Yi and Tao Cui (2011). Interference mitigaion between femtocell and macrocell. In Proceedings of 2011 International Conference on Electronics and Optoelectronics, volume 2, pages V2–102–V2–104. IEEE.

[79] Luby, M. (2002). LT codes. In The 43rd Annual IEEE Symposium on Foundations of Computer Science, 2002. Proceedings., pages 271–280. IEEE Comput. Soc.

[80] Lucani, D. E., Medard, M., and Stojanovic, M. (2009). Random Linear Network Coding for Time-Division Duplexing: Field Size Considerations. In GLOBECOM 2009 - 2009 IEEE Global Telecommunications Conference, pages 1–6. IEEE.

[81] MacKay, D. (2005). Fountain codes. IEE Proceedings - Communications, 152(6):1062.

[82] Masao Nakagawa (2007). Visible Light Communications Consortium (VLCC).

[83] Masuda, K., Kamakura, K., and Yamazato, T. (2016). Spatial modulation in layered space-time coding for image-sensor-based visible light communication. In 2016 IEEE 27th

Annual International Symposium on Personal, Indoor, and Mobile Radio Communications (PIMRC), pages 1–6. IEEE.

[84] Matsumoto, M. and Nishimura, T. (1998). Mersenne twister: a 623- dimensionally equidistributed uniform pseudo-random number generator. ACM Transactions on Modeling and Computer Simulation, 8(1):3–30.

[85] Mostafa, A. (2017). Physical-layer security for visible-light communication systems. Physical-layer security for visible-light communication systems, (April).

[86] Musa, A., Baba, M. D., and Haji Mansor, H. M. A. (2014). The design and implementation of IEEE 802.15.7 module with ns-2 simulator. In 2014 International Conference on Computer, Communications, and Control Technology (I4CT), number I4ct, pages 111–115. IEEE.

[87] Nazir, S., Vukobratovic, D., and Stankovic, V. (2011). Performance evaluation of Raptor and Random Linear Codes for H.264/AVC video transmission over DVB-H networks. In 2011 IEEE International Conference on Acoustics, Speech and Signal Processing (ICASSP), pages 2328–2331. IEEE.

[88] Nguyen, D., Tran, T., Nguyen, T., and Bose, B. (2009). Wireless broadcast using network coding. IEEE Transactions on Vehicular Technology, 58(2):914–925.

[89] Nguyen, D. T. and Park, Y. (2017). Data rate enhancement of optical camera communications by compensating inter-frame gaps. Optics Communications, 394:56–61.

[90] Nguyen, T. and Jang, Y. M. (2015). High-speed asynchronous Optical Camera Communication using LED and rolling shutter camera. In 2015 Seventh International Conference on Ubiquitous and Future Networks, pages 214–219. IEEE.

[91] Omega (2010). Home Gigabit Access (OMEGA).

[92] Otsu, N. (1979). A Threshold Selection Method from Gray-Level Histograms. IEEE Transactions on Systems, Man, and Cybernetics, 9(1):62–66.

[93] Ozekici, S. (1997). Markov modulated Bernoulli process. Mathematical Methods of Operations Research, 45(3):311–324.

[94] Paul, T. and Ogunfrunmiri, T. (2008). Wireless LAN Comes of Age: Understanding the IEEE 802.11n Amendment. IEEE Circuits and Systems Magazine, 8(1):28–54.

[95] Perli, S. D., Ahmed, N., and Katabi, D. (2010). PixNet. In Proceedings of the sixteenth annual international conference on Mobile computing and networking - MobiCom '10, page 137, New York, New York, USA. ACM Press.

[96] PureLifim (2018). pureLiFi.

[97] Rahaim, M., Vegni, A., and Little, T. (2011). A hybrid Radio Frequency and broadcast Visible Light Communication system. In 2011 IEEE GLOBECOM Workshops, GC Wkshps 2011, pages 792–796.

[98] Rajagopal, N., Lazik, P., and Rowe, A. (2014a). Hybrid visible light communication for cameras and low-power embedded devices. In VLCS '14 Proceedings of the 1st ACM MobiCom workshop on Visible light communication systems, pages 33–38.

[99] Rajagopal, N., Lazik, P., and Rowe, A. (2014b). Visual light landmarks for mobile devices. In IPSN-14 Proceedings of the 13th International Symposium on Information Processing in Sensor Networks, volume 32, pages 249–260. IEEE.

[100] Rajagopal, S., Roberts, R., and Lim, S.-K. (2012). IEEE 802.15.7 visible light communication: modulation schemes and dimming support. IEEE Communications Magazine, 50(3):72–82.

[101] Ravi, N., Scott, J., Han, L., and Iftode, L. (2008). Context-aware Battery Management for Mobile Phones. In 2008 Sixth Annual IEEE International Conference on Pervasive Computing and Communications (PerCom), pages 224–233. IEEE.

[102] Roberts, R. D. (2013a). A MIMO protocol for camera communications (CamCom) using undersampled frequency shift ON-OFF keying (UFSOOK). 2013 IEEE Globecom Workshops, GC Wkshps 2013, pages 1052– 1057.

[103] Roberts, R. D. (2013b). Undersampled frequency shift ON-OFF keying (UFSOOK) for camera communications (CamCom). In 2013 22nd Wireless and Optical Communication Conference, pages 645–648. IEEE.

[104] Roberts, R. D., Rajagopal, S., and Lim, S.-K. (2011). IEEE 802.15.7 physical layer summary. In 2011 IEEE GLOBECOM Workshops (GC Wkshps), pages 772–776. IEEE.

[105] Ryu, W. J. and Shin, S. Y. (2017). RGB MIMO optical camera communication with Histogram equalization. In 2017 International Conference on Signals and Systems (ICSigSys), pages 303–307. IEEE.

[106] Schmid, S., Arquint, L., and Gross, T. R. (2016). Using smartphones as continuous receivers in a visible light communication system. Proceedings of the 3rd Workshop on Visible Light Communication Systems - VLCS ’16, pages 61–66.

[107] Schmid, S., Corbellini, G., Mangold, S., and Gross, T. R. (2012). An LED-to-LED Visible Light Communication system with software-based synchronization. In 2012 IEEE Globecom Workshops, pages 1264–1268. IEEE.

[108] Schmid, S., Corbellini, G., Mangold, S., and Gross, T. R. (2013). LEDto-LED visible light communication networks. In Proceedings of the fourteenth ACM international symposium on Mobile ad hoc networking and computing - MobiHoc ’13, page 1, New York, New York, USA. ACM Press.

[109] Schmid, S., Schwyn, D., Aks, K., Corbellini, G., Gross, T. R., and Mangold, S. (2014). From Sound to Sight: Using Audio Processing to enable Visible Light Communication. 5th IEEE Workshop on Optical Wireless Communications (OWC’14), (Section III).

[110] Shao, S., Khreishah, A., Rahaim, M., Elgala, H., Ayyash, M., Little, T., and Wu, J. (2015). An indoor hybrid WiFi-VLC internet access system. In Proceedings - 11th IEEE International Conference on Mobile Ad Hoc and Sensor Systems, MASS 2014, pages 569–574.